Variable shortening rates in the eastern Himalayan thrust belt, Bhutan: Insights from multiple thermochronologic and geochronologic data sets tied to kinematic reconstructions

Sean P. Long,[1] Nadine McQuarrie,[2] Tobgay Tobgay,[3] Isabelle Coutand,[4] Frances J. Cooper,[5] Peter W. Reiners,[6] Jo-Anne Wartho,[5] and Kip V. Hodges[5]

Received 17 May 2012; revised 28 August 2012; accepted 31 August 2012; published 9 October 2012.

[1] We present data on the burial, displacement and exhumation history of the Himalayan fold-thrust belt in eastern Bhutan. These data document the magnitude and timing of displacement of large, discrete structures and highlight temporal variability in shortening rates. Eight new $^{40}Ar/^{39}Ar$ ages from white mica, 32 new zircon (U-Th)/He ages, 7 new apatite fission track ages, and 1 new U-Pb zircon (LA-MC-ICP-MS) metamorphic rim growth age are combined with published cooling ages and deformation temperatures, and incremental shortening magnitudes from restorations of two published balanced cross sections, to illustrate the kinematic and temporal development of the Bhutan thrust belt. Integrating these data from ~23 Ma to the present illustrates rapid horizontal shortening rates (28–35 mm/yr) between 23–20 Ma and 15–10 Ma, separated by more moderate rates (10–23 mm/yr). Shortening rates decrease significantly to 7–10 mm/yr (and possibly as low as 3–4 mm/yr) from 10 to 0 Ma. This decrease is interpreted to represent the onset of strain partitioning in the eastern part of the Himalayan-Tibetan orogenic system, between shortening in the Bhutan thrust belt, uplift of the Shillong Plateau, and deformation and outward growth of the northern and eastern Tibetan Plateau. Within estimated error, horizontal shortening rates during emplacement of the Main Central thrust sheet and during construction of the upper Lesser Himalayan duplex approached India-Asia tectonic velocities. Thus, for periods of time between ~23–20 Ma and ~15–10 Ma, the Bhutan thrust belt may have absorbed nearly all India-Asian convergence at this longitude.

Citation: Long, S. P., N. McQuarrie, T. Tobgay, I. Coutand, F. J. Cooper, P. W. Reiners, J.-A. Wartho, and K. V. Hodges (2012), Variable shortening rates in the eastern Himalayan thrust belt, Bhutan: Insights from multiple thermochronologic and geochronologic data sets tied to kinematic reconstructions, *Tectonics*, *31*, TC5004, doi:10.1029/2012TC003155.

1. Introduction

[2] Crustal shortening within the Himalayan thrust belt has played a major role in accommodating convergence between the Indian and Asian plates [e.g., *Gansser*, 1964; *LeFort*, 1975; *Hodges*, 2000; *Yin*, 2006]. However, shortening rates in the thrust belt have only been estimated at the shortest (Global Positioning System (GPS)) and longest (total shortening) timescales, with a few studies that document Holocene shortening rates [*Lavé and Avouac*, 2000; *Mugnier et al.*, 2004]. Modern convergence rates estimated by GPS studies range from ~15–20 mm/yr in the western and central Himalaya [*Bilham et al.*, 1997; *Larson et al.*, 1999; *Banerjee and Burgmann*, 2002; *Zhang et al.*, 2004; *Bettinelli et al.*, 2006] to as high as ~20–25 mm/yr in the eastern Himalaya [*Banerjee et al.*, 2008], accounting for roughly 40–60% of the ~4 cm/yr modern India-Asian convergence rate [e.g., *Copley et al.*, 2010; *van Hinsbergen et al.*, 2011]. Long-term shortening rates from ~25 Ma to present have been estimated by studies utilizing retrodeformable balanced cross sections. These studies estimate that between ~400 and 670 km of crustal shortening has been accommodated by the Himalayan thrust belt [*DeCelles et al.*, 2002; *Long et al.*, 2011b] in the last 23–25 Myr, indicating long-

[1]Nevada Bureau of Mines and Geology, University of Nevada, Reno, Reno, Nevada, USA.
[2]Department of Geology and Planetary Science, University of Pittsburgh, Pittsburgh, Pennsylvania, USA.
[3]Department of Geological Sciences, University of Texas at El Paso, El Paso, Texas, USA.
[4]Department of Earth Sciences, Dalhousie University, Halifax, Nova Scotia, Canada.
[5]School of Earth and Space Exploration, Arizona State University, Tempe, Arizona, USA.
[6]Department of Geosciences, University of Arizona, Tucson, Arizona, USA.

Corresponding author: S. P. Long, Nevada Bureau of Mines and Geology, University of Nevada, Reno, Mail Stop 178, Reno, NV 89557, USA. (splong@unr.edu)

0278-7407/12/2012TC003155

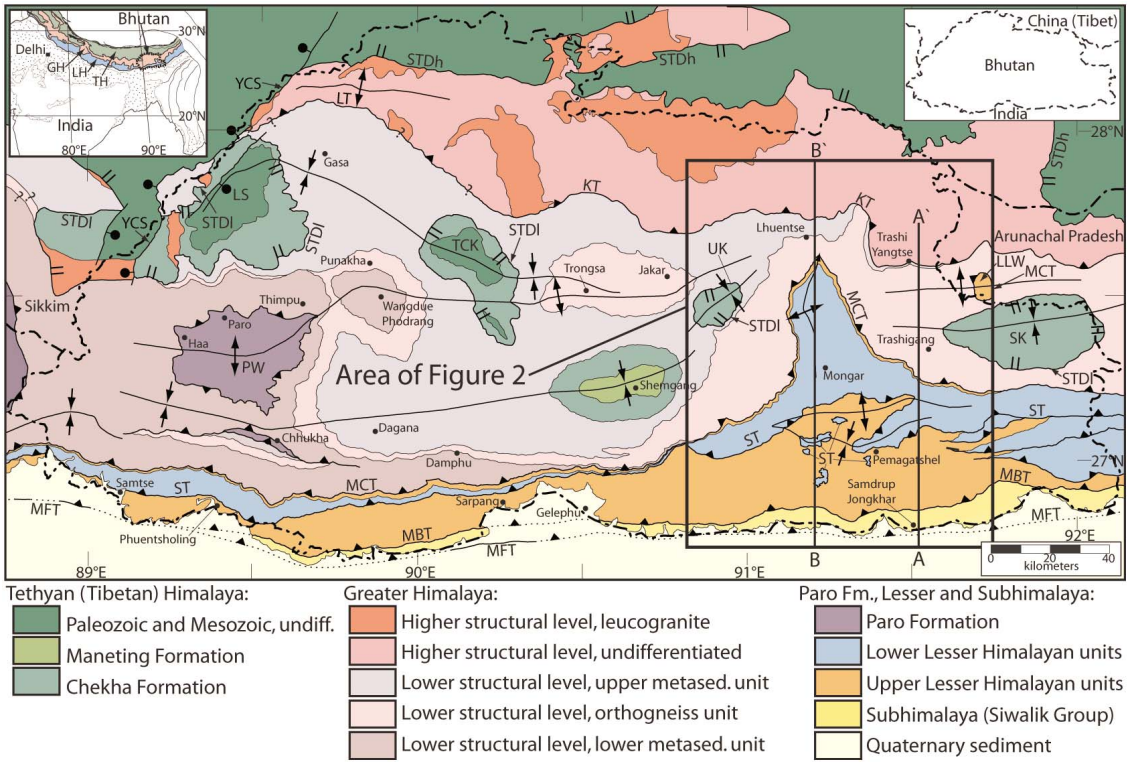

Figure 1. Simplified geologic map of Bhutan and surrounding region, after *Long et al.* [2011d]. Area of Figure 2 shown, along with lines of section of the Kuru Chu (B-B′) and Trashigang (A-A′) cross sections (Figure 3). Top left inset shows a generalized geologic map of the central and eastern Himalayan orogen (modified from *Gansser* [1983]). Abbreviations (1) in inset are GH: Greater Himalaya, LH: Lesser Himalaya, TH: Tethyan Himalaya: (2) structures from north to south: YCS: Yadong Cross-Structure, STDh: structurally higher South Tibetan detachment, LT: Laya thrust, KT: Kakhtang thrust, STDl: structurally lower South Tibetan detachment, MCT: Main Central thrust, ST: Shumar thrust MBT: Main Boundary thrust, MFT: Main Frontal thrust; (3) windows and klippen from west to east: LS: Lingshi syncline, PW: Paro window, TCK: Tang Chu klippe, UK: Ura klippe, SK: Sakteng klippe, LLW: Lum La window.

term shortening rates between 16 and 29 mm/yr. The agreement between long-term rates and GPS rates has led to the prevailing assumption that the motion rate along the basal décollemont of the thrust belt (the Main Himalayan thrust) has been constant through time [e.g., *Herman et al.*, 2010]. However, petrologic, geochronologic, and structural studies focused on major structures that have accommodated a large percentage of total Himalayan shortening, such as the Main Central Thrust and Ramgarh thrust, have argued for large variations in Himalayan shortening rates, by factors as high as 2–3, at Myr timescales [e.g., *Kohn et al.*, 2004; *Tobgay et al.*, 2012]. These observations invalidate the assumption of constant Himalayan shortening rates, and imply that variable shortening rates may be the rule rather than the exception for Himalayan deformation. Thus, although the long-term shortening rates estimated from cross-section studies are similar to GPS rates, they may represent the average of periods of faster and slower shortening. Understanding the variability in shortening rates, and interpreting these variations in the context of the greater Himalayan-Tibetan orogenic system, requires documentation of incremental shortening rates over the full period of activity of the Himalayan thrust belt.

[3] In this study, we utilize multiple thermochronologic systems to obtain cooling histories for Himalayan thrust sheets in eastern Bhutan (Figure 1), and we combine these data with published cooling ages, deformation and peak temperatures, and prograde metamorphic ages. By integrating these data sets with sequential restorations of two balanced cross sections, we are able to quantify a detailed record of the burial, displacement, and exhumation history of the thrust belt, and to constrain a four-part record of Himalayan shortening rates between ~23 Ma and the present. Our results highlight significant temporal variability in shortening rates, which we place in the larger temporal and spatial framework of deformation not just in the Himalayan thrust belt, but in all major components of the greater Himalayan-Tibetan Plateau orogenic system. These results have important implications for the temporal history and magnitude of strain partitioning in the eastern part of the orogen.

2. Himalayan Geologic Background

[4] The Himalayan-Tibetan Plateau orogenic system is the first-order expression of Tertiary collision and continued convergence between the Indian and Eurasian plates [*Heim*

and Gansser, 1939; *Gansser*, 1964; *LeFort*, 1975; *Hodges*, 2000]. The south vergent Himalayan fold-thrust belt forms the southern part of the orogenic system, and is composed of thrust sheets of Paleoproterozoic to Quaternary sedimentary, metasedimentary, and igneous rocks [*Gansser*, 1964; *Powell and Conaghan*, 1973; *LeFort*, 1975; *Mattauer*, 1986; *Hodges*, 2000; *DeCelles et al.*, 2002; *Yin*, 2006]. The Himalayan thrust belt is divided into four tectonostratigraphic zones (Figure 1), the Subhimalaya (SH), Lesser Himalaya (LH), Greater Himalaya (GH), and Tethyan Himalaya (TH) [*Heim and Gansser*, 1939; *Gansser*, 1964]. The LH, GH, and TH zones are packages of pre-Himalayan sedimentary and igneous rocks of Greater India that have been metamorphosed to varying extents during Himalayan orogenesis, and the SH zone represents synorogenic deposition in the Himalayan foreland basin. The SH zone is thrust over modern foreland basin sediments across the Main Frontal thrust (MFT), the LH zone is thrust over the SH zone across the Main Boundary thrust (MBT), and the GH zone is thrust over the LH zone across the Main Central thrust (MCT) [*Heim and Gansser*, 1939; *Gansser*, 1964]. In most places, the TH zone sits structurally above the GH zone across the normal-sense South Tibetan Detachment (STD) system [*Burg*, 1983; *Burchfiel et al.*, 1992], but in several localities the GH-TH contact is interpreted as stratigraphic [*Stocklin*, 1980; *Gehrels et al.*, 2003; *Robinson et al.*, 2006; *Long and McQuarrie*, 2010].

3. The Himalayan Thrust Belt in Bhutan

3.1. Lesser Himalayan and Subhimalayan Zones

[5] The LH zone in eastern Bhutan consists of six map units [*Long et al.*, 2011a]. From oldest to youngest, they are the Shumar and Daling formations, which comprise the Paleoproterozoic Daling-Shumar Group, which we refer to as the lower LH section, and the Neoproterozoic-Cambrian (?) Baxa Group, Neoproterozoic-Ordovician(?) Jaishidanda Formation, Permian Diuri Formation, and Permian Gondwana succession, which we refer to as the upper LH section.

[6] The Paleoproterozoic Daling-Shumar Group displays a two-part stratigraphy of quartzite of the Shumar Formation below schist, phyllite, and quartzite of the Daling Formation [*McQuarrie et al.*, 2008; *Long et al.*, 2011a]. The upper contact of the Daling-Shumar Group is an unconformity with quartzite and schist of the Neoproterozoic-Ordovician Jaishidanda Formation [*Long et al.*, 2011a]. The combined Daling-Shumar Group and Jaishidanda Formation sections are structurally repeated in the lower LH duplex system, with the Shumar thrust (ST) acting as the floor thrust and the MCT acting as the roof thrust [*Long et al.*, 2011b].

[7] The Neoproterozoic-Cambrian Baxa Group consists of interbedded quartzite, phyllite, and dolomite [*McQuarrie et al.*, 2008; *Long et al.*, 2011a]. Multiple ~1.5–2.5 km thick horses of the Baxa Group are structurally repeated in the upper LH duplex system, with the ST acting as the roof thrust [*Long et al.*, 2011b]. The Permian Diuri Formation consists of pebble-clast diamictite, and the Permian Gondwana succession consists of sandstone, carbonaceous siltstone and shale, and coal [*McQuarrie et al.*, 2008; *Long et al.*, 2011a]. These Permian LH units are carried in single thrust sheets in southeast Bhutan, the southernmost being the MBT sheet (Figures 2 and 3) [*Long et al.*, 2011b].

[8] The SH zone consists of siltstone, sandstone, and conglomerate of the Miocene-Pliocene Siwalik Group [*Long et al.*, 2011a]. The SH zone consists of a single thrust sheet, uplifted along the MFT (Figures 2 and 3) [*Long et al.*, 2011b].

3.2. Greater and Tethyan Himalayan Zones

[9] The GH zone in Bhutan is divided into a lower structural level above the MCT and below the Kakhtang thrust (KT), and locally below a structurally lower level of the South Tibetan detachment (STDl), and a higher structural level between the KT and a structurally higher level of the South Tibetan detachment (STDh) (Figures 1 and 3) [*Grujic et al.*, 2002]. The structurally higher GH section is up to ~13 km thick, and consists of migmatitic orthogneiss and metasedimentary rocks, intruded by Miocene leucogranite (Figure 1) [*Gansser*, 1983; *Swapp and Hollister*, 1991; *Davidson et al.*, 1997; *Grujic et al.*, 2002; *Long et al.*, 2011d]. The structurally lower GH section is ~8 km thick in eastern Bhutan, and consists of a lower, Cambrian-Ordovician granitic orthogneiss unit and an upper metasedimentary unit, composed of quartzite, schist, phyllite, and paragneiss [*Long and McQuarrie*, 2010; *Long et al.*, 2011b, 2011d] (Figure 1). Rocks above and below the MCT and KT exhibit hanging wall flat over footwall flat relationships, indicating that the hanging wall cutoffs for both GH sections have passed through the erosion surface [*Long et al.*, 2011b]. The structurally lower GH section exhibits regional-scale, east-west trending antiforms and synforms, which are attributed to growth of the underlying lower LH duplex [*Long et al.*, 2011b].

[10] In eastern Bhutan, isolated exposures of greenschist facies metasedimentary rocks of the TH zone lie above the GH section in the axes of two synforms (Figure 2) [*Gansser*, 1983; *Bhargava*, 1995; *Edwards et al.*, 1996; *Grujic et al.*, 2002; *Long et al.*, 2011b, 2011d]. These rocks consist of quartzite and schist of the Chekha Formation, the basal TH unit. These are the easternmost of five isolated TH exposures in Bhutan (Figure 1). Four of the five isolated TH exposures have been interpreted as klippen above the STDl [*Grujic et al.*, 2002], based on field evidence for top-to-the-north sense shear zones at the base of the Chekha Formation. However, in the Shemgang region in central Bhutan, the Chekha Formation is in interfingering depositional contact above GH metasedimentary rocks [*Long and McQuarrie*, 2010]. No identifiable stratigraphic offset below or within the TH section [*Long and McQuarrie*, 2010], combined with minimal to diffuse changes in pressure or temperature along potential structural boundaries [*Kellett and Grujic*, 2012], makes documenting the exact amount of displacement on the STDl, and how this amount may change along strike, difficult. Normal-sense displacement estimates on this structure range from 20 to 65+ km [*Long and McQuarrie*, 2010; *Cooper et al.*, 2012].

4. Thermochronology Data

4.1. White Mica $^{40}Ar/^{39}Ar$ Data

[11] We present eight new $^{40}Ar/^{39}Ar$ ages from white mica (MAr) from LH rocks collected on the Kuru Chu transect (Figure 2). Analyses were performed at the Arizona State University Noble Gas Geochronology and Geochemistry

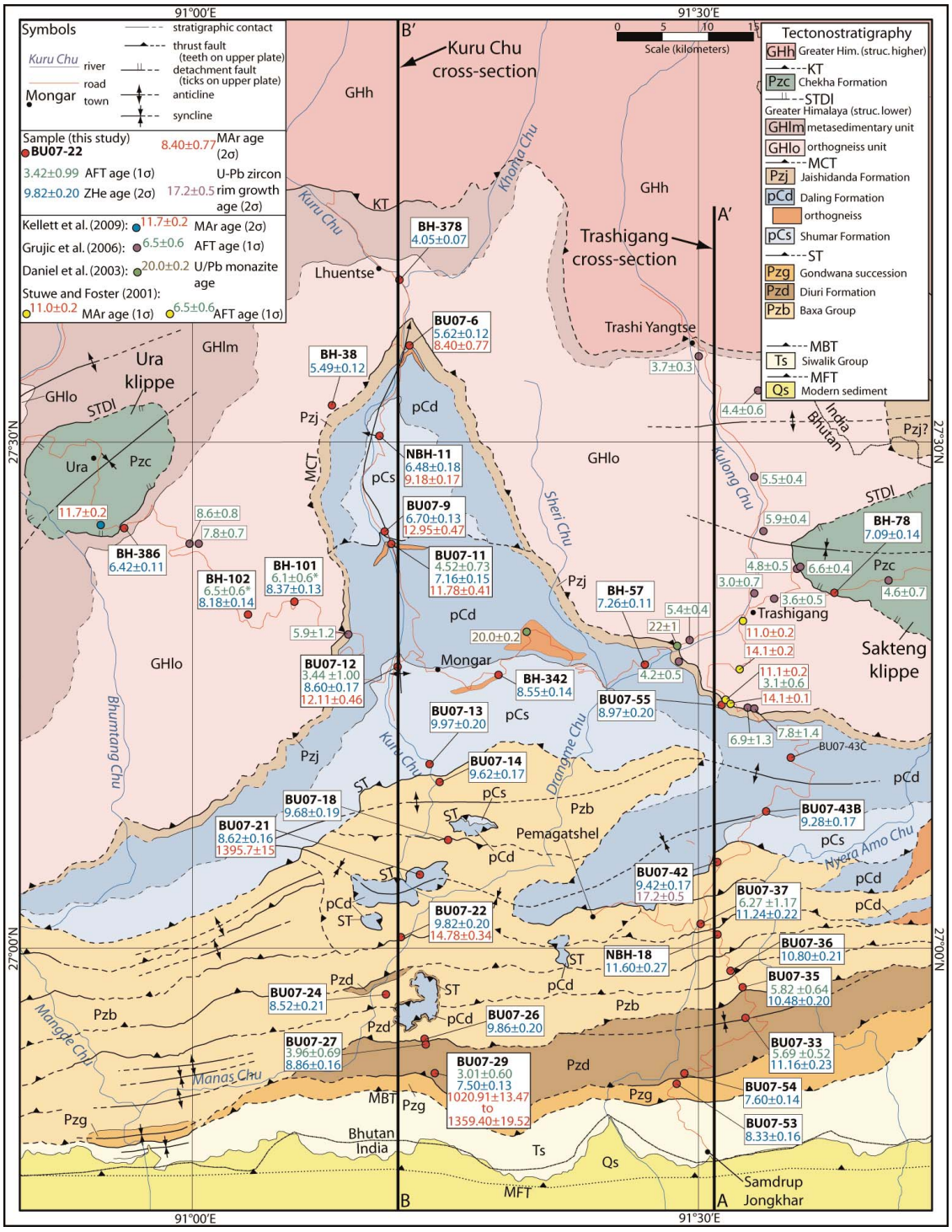

Figure 2. Geologic map of part of eastern Bhutan, simplified from *Long et al.* [2011b]. See Figure 1 caption for structure abbreviations. Lines of section of Kuru Chu (B-B′) and Trashigang (A-A′) cross sections (Figure 3) are shown. Red circles mark locations of thermochronology samples from this study. Red ages are MAr, blue ages are ZHe, green ages are AFT, and single purple age is U-Pb zircon metamorphic rim growth age. Purple circles mark AFT ages from *Grujic et al.* [2006], yellow circles mark MAr and AFT ages from *Stüwe and Foster* [2001], blue circle marks MAr age from *Kellett et al.* [2009], and green circles mark U-Pb monazite ages from *Daniel et al.* [2003]. AFT ages marked with asterisks (BH-101, BH-102) were published by *Grujic et al.* [2006], and new ZHe ages from the same two samples are presented here.

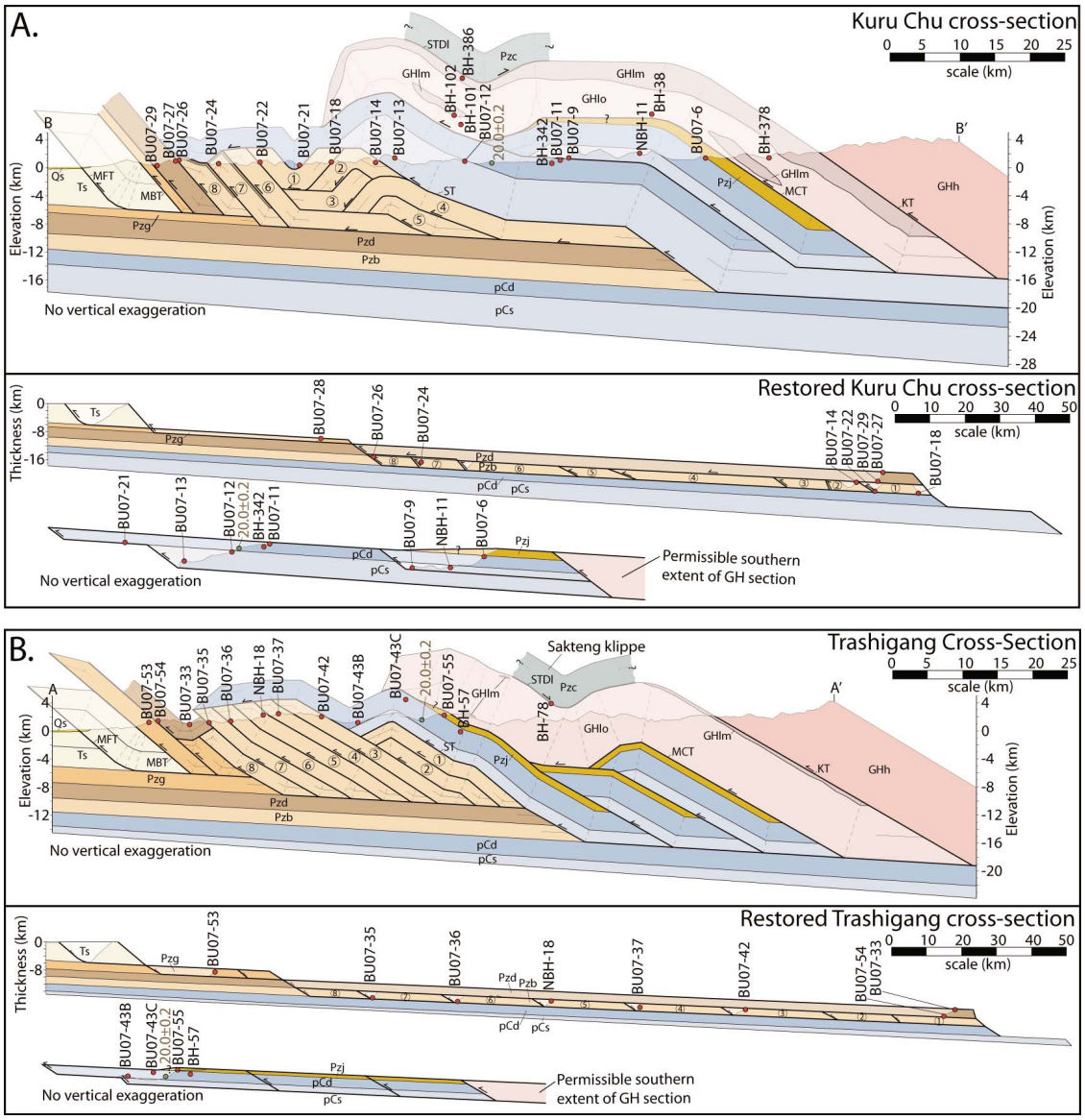

Figure 3. Deformed and restored balanced cross sections along the (a) Kuru Chu and (b) Trashigang transects (simplified from Figure 3 of *Long et al.* [2011b]). Lines of section are shown on Figures 1 and 2. Restored sections are shown at a smaller scale than deformed sections. Translucent areas represent rock that has passed above the modern erosion surface. See Figure 2 for unit abbreviations, and see Figure 1 caption for structure abbreviations. Deformed and restored locations of thermochronology samples from this study (red circles) are shown. The 20.0 ± 0.2 Ma age (U-Pb monazite) shows projected position of the LH orthogneiss sample dated by *Daniel et al.* [2003]. Baxa Group horses are numbered in the order in which they were emplaced.

Laboratories; see Text S1, section 2, in the auxiliary material for discussion of methods.[1] Final interpreted MAr ages for each sample are reported with 2σ error on Table 1 and Figure 2, the data used in interpretation of these ages are shown in Table 2, and age spectra plots from five samples are shown in Figure 4. Supporting data for MAr analyses are shown in Table S1, and additional age spectra and inverse isochron plots are shown in Figure S1.

[12] Three samples were analyzed from structurally high (BU07-6), medium (NBH-11), and low (BU07-9) positions within the northernmost lower LH thrust sheet. Samples BU07-6 and BU07-9 yielded integrated ages (the average of all heating steps, which yields the equivalent of a total fusion age) of 8.40 ± 0.77 Ma (BU07-6) and 12.95 ± 0.47 Ma (BU07-9), and sample NBH-11 yielded a plateau age of 9.18 ± 0.17 Ma (Figure 4a). These three samples show a trend of increasing MAr age toward the south (Figure 2). Two samples were analyzed from structurally high (BU07-11) and medium (BU07-12) positions within the ST sheet, and

[1]Auxiliary materials are available in the HTML. doi:10.1029/2012TC003155.

Table 1. Sample Locations and Cooling Ages From Eastern Bhutan

Sample	Latitude	Longitude	Elevation (m)	Map Unit	Lithology	MAr Age (Ma)	MAr 2σ Error (Ma)	ZHe Age (Ma)	ZHe 2σ Error (Ma)	Number of Zircons Analyzed	AFT Age (Ma)	AFT 1σ Error (Ma)	U-Pb Zircon Rim Growth Age (Ma); $\pm 2\sigma$
					Kuru Chu Cross Section								
BH-378	91.20487	27.66549	1195	Greater Him.	paragneiss	-	-	4.05	0.07	3	-	-	-
BH-38	91.14425	27.54036	2145	Greater Him.	paragneiss	-	-	5.49	0.12	2	-	-	-
BH-386	90.93286	27.41050	3520	Greater Him.	paragneiss	-	-	6.42	0.11	3	-	-	-
BH-102	91.05517	27.32900	2795	Greater Him.	paragneiss	-	-	8.18	0.14	3	-	-	-
BH-101	91.10072	27.34133	2380	Greater Him.	orthogneiss	-	-	8.37	0.13	3	-	-	-
BU07-6	91.21519	27.59367	1170	Jaishidanda	quartzite	8.40	0.77	5.62	0.12	3	-	-	-
NBH-11	91.18354	27.50625	1365	Shumar	quartzite	9.18	0.17	6.48	0.18	2	-	-	-
BU07-9	91.18111	27.40256	930	Shumar	quartzite	12.95	0.47	6.70	0.13	3	-	-	-
BU07-11	91.19339	27.39969	840	Daling	orthogneiss	11.78	0.41	7.16	0.15	3	4.52	0.73	-
BU07-12	91.20289	27.27808	995	Shumar	quartzite	12.11	0.46	8.60	0.17	3	3.44	1.00	-
BH-342	91.29907	27.26742	2210	Shumar	orthogneiss	-	-	8.55	0.14	3	-	-	-
BU07-13	91.23342	27.18844	645	Shumar	quartzite	-	-	9.97	0.20	3	-	-	-
BU07-14	91.24000	27.16608	600	Baxa	quartzite	-	-	9.62	0.17	3	-	-	-
BU07-18	91.25686	27.10706	1580	Baxa	quartzite	-	-	9.68	0.19	3	-	-	-
BU07-21	91.22197	27.07247	950	Daling	quartzite	1395.7	15	8.62	0.16	3	-	-	-
BU07-22	91.20628	27.00844	260	Baxa	quartzite	14.78	0.34	9.82	0.20	3	-	-	-
BU07-24	91.19019	26.95358	505	Baxa	quartzite	-	-	8.52	0.21	2	-	-	-
BU07-26	91.22817	26.90828	975	Baxa	quartzite	-	-	9.86	0.20	3	-	-	-
BU07-27	91.23072	26.90567	975	Diuri	diamictite	-	-	8.86	0.16	3	3.96	0.69	-
BU07-29	91.23983	26.87803	465	Diuri	diamictite	1020.91	13.47	7.50	0.13	3	3.01	0.60	-
					Trashigang Cross Section								
BH-78	91.63897	27.35144	1000	Chekha	schist	-	-	7.09	0.14	2	-	-	-
BU07-55	91.52122	27.24222	2350	Jaishidanda	quartzite	-	-	8.97	0.20	2	-	-	-
BH-57	91.44656	27.27869	605	Daling	quartzite	-	-	7.26	0.11	3	-	-	-
BU07-43B	91.56708	27.13450	2315	Daling	quartzite	-	-	9.28	0.17	3	-	-	-
BU07-42	91.52089	27.08486	2165	Baxa	quartzite	-	-	9.42	0.17	3	-	-	17.2 $\pm$ 0.5
BU07-37	91.50142	27.02675	2385	Baxa	quartzite	-	-	11.24	0.22	3	6.27	1.17	-
NBH-18	91.52072	27.01200	1815	Baxa	quartzite	-	-	11.60	0.27	2	-	-	-
BU07-36	91.53083	26.97442	1785	Baxa	quartzite	-	-	10.80	0.21	3	-	-	-
BU07-35	91.54761	26.95992	1580	Baxa	quartzite	-	-	10.48	0.20	3	5.82	0.64	-
BU07-33	91.54794	26.93311	1710	Diuri	diamictite	-	-	11.16	0.23	3	5.69	0.52	-
BU07-54	91.48028	26.87497	700	Diuri	quartzite	-	-	7.60	0.14	3	-	-	-
BU07-53	91.48011	26.86572	655	Gondwana	sandstone	-	-	8.33	0.16	3	-	-	

Table 2. White Mica $^{40}Ar/^{39}Ar$ Interpreted Results[a]

Sample Number	Integrated Age (Ma)	±Error[b]	Total Number of Steps	Plateau Age (Ma)	±Error[b]	MSWD	P	Steps	% ^{39}Ar	Isochron Age (Ma)	±Error	Initial $^{40}Ar/^{36}Ar$	±Error	MSWD	P	Steps	Minimum Age (Ma)	±Error	Maximum Age (Ma)	±Error
BU07-06	**8.40**	**0.77** (0.76)	2	-		-	-	-	-	-	-	-		-	-			-	-	-
BU07-09	**12.95**	**0.47** (0.33)	4	-		-	-	-	-	11.8	1.8	650	470	0.24	0.78	A-D		-	-	-
BU07-11	**11.78**	**0.41** (0.26)	6	-		-	-	-	-	11.43	0.58	424	86	2	0.09	A-G		-	-	-
BU07-12	**12.11**	**0.46** (0.33)	2	-		-	-	-	-	-	-	-		-	-			-	-	-
BU07-21	**1395.7**	**15** (5.7)	4	-		-	-	-	-	-	-	-		-	-		1320	16.3	1460.9	16.5
BU07-22	90.6	1.3 (0.26)	12	-		-	-	-	-	14.07	0.70	1010	600	3.1	0.01	A-H	**≤14.78**	**0.34**	**≥575.96**	**8.40**
BU07-29	1160.2	10 (4.5)	10	-		-	-	-	-	-	-	-		-	-		**≤1020.91**	**13.47**	**≥1359.40**	**19.52**
NBH-11	9.25	0.17 (0.09)	12	**9.18**	**0.17** (0.09)	0.82	0.56	F-L	58.3	9.03	0.19	380	32	1.8	0.06	A-L	-	-	-	-

[a]The sample ages shown in bold indicate our interpreted ages. All errors are quoted at 2σ. MSWD = mean squared of weighted deviates. P = probability.
[b]The quoted errors on the integrated and plateau ages are inclusive of the J value errors (the ages and errors in brackets are exclusive of the J value errors).

yielded integrated ages of 11.78 ± 0.41 Ma (BU07-11; Figure 4b) and 12.11 ± 0.46 Ma (BU07-12). Sample BU07-21, which was collected from the ST sheet in a klippe of the Daling Formation, yielded an integrated age of 1395.7 ± 15 Ma (Figure 4c), indicating that detrital white mica populations in this sample were not thermally reset during Himalayan orogenesis.

[13] Sample BU07-22, which was collected from Baxa Group horse 1 in the upper LH duplex (Figure 2), yielded a complex $^{40}Ar/^{39}Ar$ spectrum. Eight incremental heating steps (corresponding to the first ~82% of ^{39}Ar released) yielded similar apparent ages (Figure 4e), suggesting circa 15 Ma cooling through muscovite closure. Higher temperature steps show more erratic behavior with apparent ages in excess of 200 Ma (Figure 4d). One interpretation of this spectrum is that the older ages represent a mixed population of unreset (circa 575 Ma) and partially reset (circa 200–300 Ma) detrital white mica. Notably, the detrital zircon population in this sample includes a Cambrian (525 Ma) component [*Long et al.*, 2011a]. We interpret the circa 15 Ma ages as indicative of a population of neoblastic white mica. Syndeformational neoblastic white mica grains ≤0.5 mm long, primarily in pressure shadows adjacent to ductilely elongated quartz clasts, have been documented in Baxa Group quartzite and phyllite throughout eastern Bhutan [*Long et al.*, 2011c], and specifically are observed in sample BU07-22 (Figure 5).

[14] Sample BU07-29, which was collected from the Diuri Formation thrust sheet, yielded Mesoproterozoic ages between 1020.91 ± 13.47 Ma and 1359.40 ± 19.52 Ma (Table 2 and Figure 4f), which we interpret as mixed populations of detrital white mica that were not thermally reset during Himalayan orogenesis.

4.2. Zircon (U-Th)/He Data

[15] We present 32 new zircon (U-Th)/He ages (ZHe) from 26 LH samples, 5 GH samples, and 1 TH sample in eastern Bhutan (Figure 2). Analyses were performed at the University of Arizona Radiogenic Helium Dating Laboratory; see Text S1, section 3, for discussion of methods. Each age presented here is a weighted mean age of 2 to 3 single zircon grains and is reported with 2σ error (Table 1 and Figure 2). For single-grain ZHe ages and supporting data, refer to Table S2.

4.2.1. Kuru Chu Transect

[16] Five samples from the structurally lower GH section were analyzed. Sample BH-378, from the middle part of the GH section near Lhuentse, yielded an age of 4.05 ± 0.07 Ma, and sample BH-38, from the base of the GH section south of Lhuentse, yielded an age of 5.49 ± 0.12 Ma. Samples BH-101, BH-102, and BH-386 were collected at structurally low, medium, and high positions within the GH section on the road west of Mongar, and yielded 8.37 ± 0.13 Ma (BH-101), 8.18 ± 0.14 Ma (BH-102), and 6.42 ± 0.11 Ma (BH-386) ages.

[17] Samples BU07-6, NBH-11, and BU07-9 were collected at structurally high, medium, and low positions within the northernmost lower LH thrust sheet, and samples BU07-11, BH-342, BU07-12, and BU07-13 were collected at structurally high, medium, medium, and low positions within the ST sheet. These seven samples show a consistent trend of increasing ZHe age toward the south, from 5.62 to 9.97 Ma (Figure 2). A sample from the base of the ST sheet in a

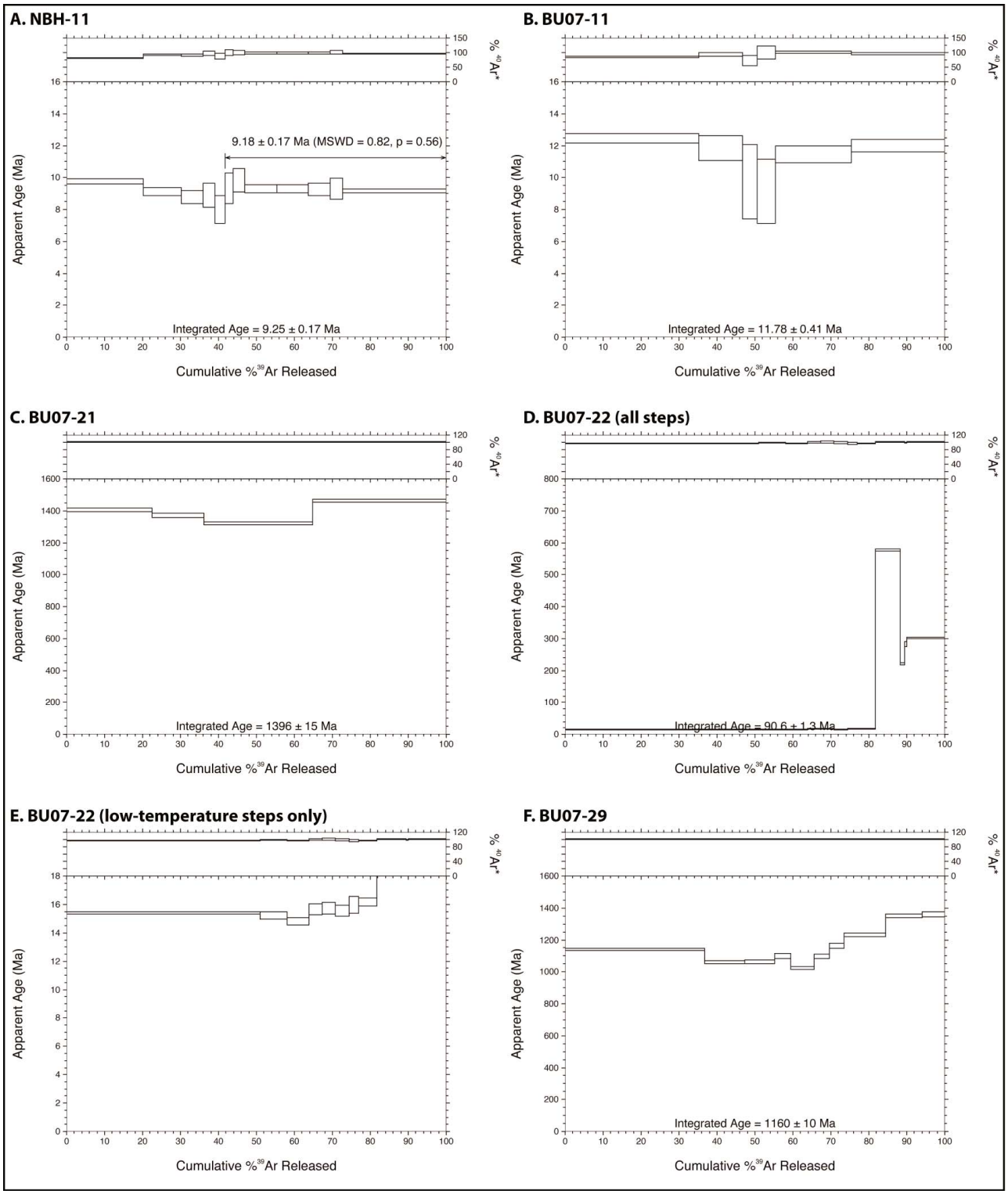

Figure 4. The $^{40}Ar/^{39}Ar$ age spectra plots for five LH samples from the Kuru Chu transect. Two plots are included for sample BU07-22, including one showing all heating steps and one showing only low-temperature steps. Refer to Tables 2 and S1 for supporting data and Figure S1 for additional age spectra and inverse isochron plots.

klippe of the Daling Formation (BU07-21) yielded an age of 8.62 ± 0.16 Ma.

[18] Five Baxa Group samples were collected from four different horses in the upper LH duplex, and four out of five samples yielded ages between 9.62 and 9.86 Ma, with one outlier at 8.62 Ma (Figure 2). Two samples were analyzed from structurally high (BU07-27) and low (BU07-29)

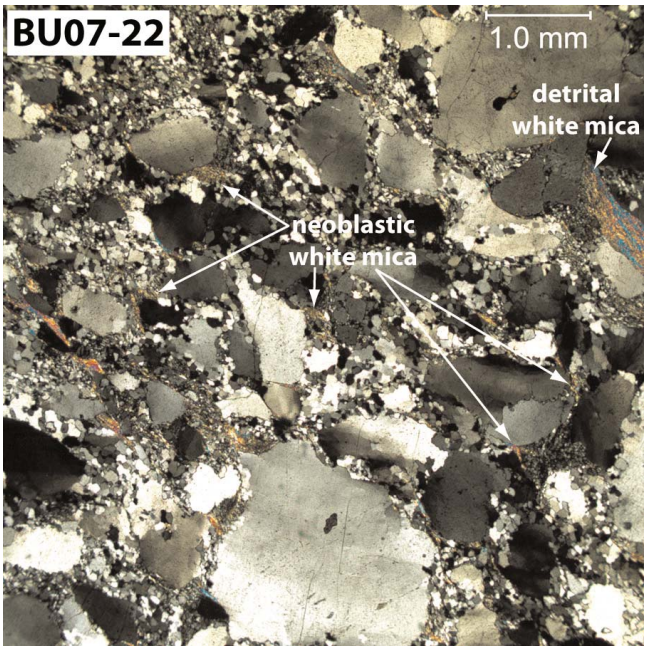

Figure 5. Photomicrograph of Baxa Group sample BU07-22, in cross-polarized light, illustrating two distinct populations of white mica, including large (≥1.0 mm) detrital mica grains, and small (typically 0.10–0.25 mm) neoblastic, syndeformational mica grains, which grow in strain shadows between ductilely elongated quartz grains [*Long et al.*, 2011c]. Quartzite bedding is parallel to the upper and lower edges of the photo. Quartz recrystallization microstructure is characteristic of the transition from bulging to subgrain rotation crystallization, indicating a deformation temperature of ~400°C [*Stipp et al.*, 2002].

positions in the Diuri Formation thrust sheet, and yielded 8.86 ± 0.16 and 7.50 ± 0.13 Ma ages.

4.2.2. Trashigang Transect

[19] One sample of the Chekha Formation (BH-78), collected just above the STDl east of Trashigang, yielded an age of 7.09 ± 0.14 Ma. Samples BU07-55, BH-57, and BU07-43B were collected from structurally high, medium, and low positions in the ST sheet, and yielded 8.97 ± 0.20 Ma, 7.26 ± 0.11 Ma, and 9.28 ± 0.17 Ma ages, respectively.

[20] Five Baxa Group samples were collected from five different horses in the upper LH duplex, and four out of five samples yielded ages between 10.48 and 11.60 Ma, with one outlier at 9.42 Ma (Figure 2). Two samples were analyzed from structurally high (BU07-33) and low (BU07-54) positions within the Diuri Formation thrust sheet, and yielded 11.16 ± 0.23 Ma and 7.60 ± 0.14 Ma ages. One sample was analyzed from the Gondwana succession in the MBT sheet (BU07-53), and yielded an age of 8.33 ± 0.16 Ma.

4.3. Apatite Fission Track Data

[21] We present 7 new apatite fission track (AFT) ages from LH rocks (Figure 2). Out of a total of 28 LH samples processed for apatite separates, only 7 yielded apatite of sufficient size and quality for reliable AFT ages. Analyses were performed at the Dalhousie University Fission Track Research Laboratory; see Text S1, section 4, for discussion of methods. AFT ages for each sample are reported with 1σ error on Table 1 and Figure 2; refer to Table S3 for supporting data.

[22] On the Kuru Chu transect, two samples were analyzed from the top (BU07-11) and middle (BU07-12) of the ST sheet, and yielded ages of 4.52 ± 0.73 Ma and 3.44 ± 1.00 Ma. Two samples were analyzed from high (BU07-27) and low (BU07-29) positions in the Diuri Formation thrust sheet and yielded ages of 3.96 ± 0.69 Ma and 3.01 ± 0.60 Ma.

[23] On the Trashigang transect, sample BU07-37 from Baxa Group horse 4 yielded an age of 6.27 ± 1.17 Ma, sample BU07-35 from Baxa Group horse 7 yielded an age of 5.82 ± 0.64 Ma, and sample BU0-33 from the Diuri Formation thrust sheet yielded an age of 5.69 ± 0.52 Ma.

4.4. Zircon U-Pb Metamorphic Rim Growth Age

[24] We collected U-Pb geochronologic analyses on individual detrital zircon grains from sample BU07-42, which was collected from Baxa Group horse 3, just below the ST on the Trashigang transect (Figures 2 and 3), using laser ablation multicollector inductively coupled plasma–mass spectrometry (LA-MC-ICP-MS) at the University of Arizona LaserChron Center. See Text S1, section 5, for discussion of methods. Concordia plots for BU07-42 are shown in Figure 6, and data from individual analyses are shown in Table S4.

[25] Individual zircon grains were mounted on two-sided tape, and the outside of 61 grains were ablated. The analyses yielded a total age range between ~1856 and ~14 Ma. The youngest coherent group of ages is defined by 17 analyses that overlap within error, which range between circa 14 and 21 Ma, and yield a weighted mean age of 17.2 ± 0.3 Ma (2σ), and 17.2 ± 0.5 Ma (2σ) after quadratic addition of systematic error (Text S1, section 5). Within this coherent group, the weighted mean of the youngest three analyses (14.9 ± 0.6 Ma [2σ], and 14.9 ± 0.7 Ma [2σ] after quadratic addition of systematic error; Text S1, section 5), defines the youngest age for growth of metamorphic zircon rims.

5. Temperature-Time Paths From Exhumation Rate Modeling

[26] To generate temperature-time (T-t) paths that quantify time-averaged exhumation rates for our samples, we performed 1-D thermal modeling [e.g., *Laslett et al.*, 1987; *Mancktelow and Grasemann*, 1997; *Ehlers and Farley*, 2003; *Thiede et al.*, 2009]. We used the AGE2EDOT program written by *Brandon et al.* [1998] to evaluate the permissible range of exhumation rates required to obtain the observed MAr, ZHe, and AFT ages, as well as a permissible range of closure temperatures for each thermochronologic age (Text S1, section 6, Table S5). Our rationale for this 1-D thermal modeling approach is based on the results of *Whipp et al.* [2007], who found that cooling ages are the most sensitive to the vertical (i.e., 1-D exhumation) component of the kinematic field in rapidly eroding orogens [e.g., *Thiede et al.*, 2009]. In addition, thermal models suggest minimal effects of thermal transients on the rapid exhumation rates typical to the Himalaya [*Ehlers et al.*, 2005; *Reiners and Brandon*, 2006]. Although this approach does not capture all of the details of the evolving thermal field, existing 2-D and

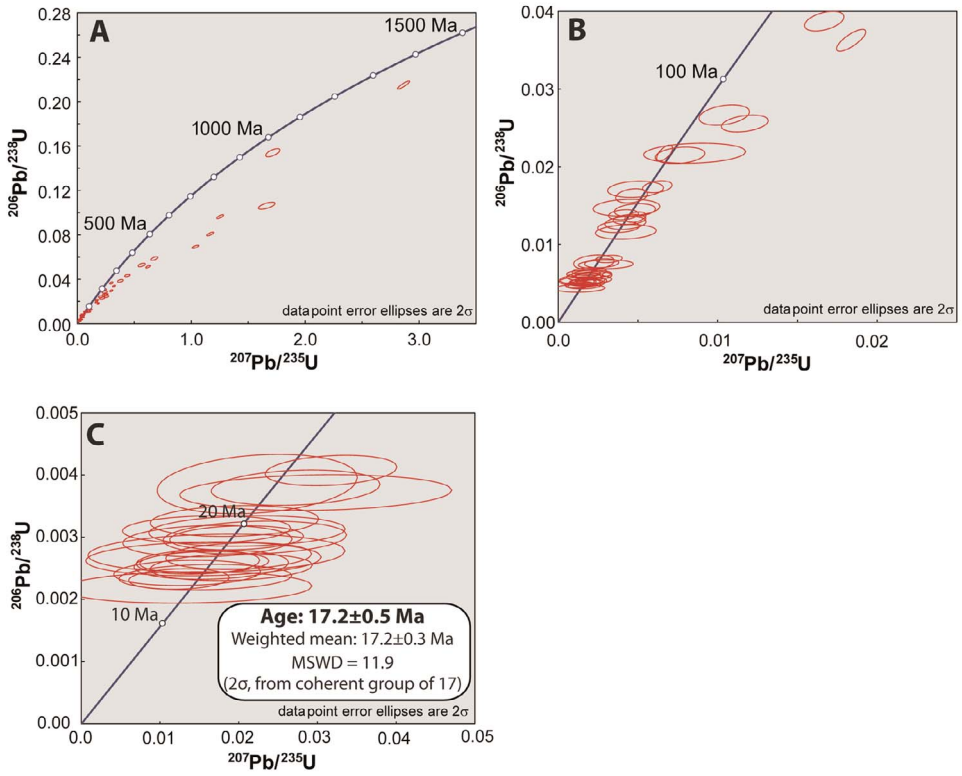

Figure 6. Pb/U concordia plots for Baxa Group sample BU07-42. Data for individual zircon analyses are listed in Table S4. Error ellipses are shown at the 2σ level (95% confidence). (a) All zircon data, and (b and c) scaled for evaluation of younger, concordant ages. In Figure 6c, the 17.2 $\pm$ 0.5 Ma age is the weighted mean of the youngest concordant group of grains that overlap within error (n = 17). The weighted mean age of the youngest 3 analyses is 14.9 $\pm$ 0.7 Ma (see Text S1, section 5).

3-D advection diffusion thermal models (1) are not designed to address potential variations in shortening rates and (2) require simplified basal thrust geometries [e.g., *Herman et al.*, 2007; 2010; *Whipp et al.*, 2007]. Examination of 1-D cooling models suggests that both variations in shortening rate as well as temporal variations in evolving geometry of the basal décollemont matters.

[27] The AGE2EDOT program determines rate-dependent cooling by solving the steady state advection diffusion equation for user-defined initial conditions and physical parameters. Physical parameters include thermal diffusivity and internal heat production, which were varied to correspond to the limits of thermal conductivity and volumetric heat production estimated for Himalayan rocks [*Ray et al.*, 2007; *Whipp et al.*, 2007; *Herman et al.*, 2010]. Initial conditions that were held constant include the layer depth to constant temperature, and average annual surface temperature. The largest variable was the geothermal gradient measured at the surface. Because data quantifying modern geothermal gradients in Bhutan are not available, we modeled our cooling data with geothermal gradients of 20, 30 and 40°C/km, to cautiously account for the effects of widely ranging geothermal gradients (Text S1, section 6, Table S5).

[28] T-t paths were constructed for each of our 32 samples, using the 7 new MAr ages, 32 new ZHe ages, and 7 new AFT ages presented here (Figure S2). T-t paths of representative samples from major structural systems, including the MCT sheet, lower LH duplex, upper LH duplex, and Diuri Formation and MBT sheets, are also shown in Figure 7. Published cooling ages from LH, GH and TH rocks in eastern Bhutan, including 15 AFT ages from *Grujic et al.* [2006], 4 MAr ages and 1 AFT age from *Stüwe and Foster* [2001], and 1 MAr age from *Kellett et al.* [2009] (Figure 2), were also utilized to augment the T-t paths for 6 of our samples, and to generate 4 additional T-t paths (Figure S2). Closure temperature ranges utilized in our T-t paths are a function of exhumation rate, composition and radiation damage [e.g., *Ketcham et al.*, 1999; *Reiners et al.*, 2004; *Flowers et al.*, 2009; *Guenthner et al.*, 2011]. Thus, AGE2EDOT closure temperatures were modified to account for variations due to composition and radiation damage. Closure temperature and diffusion parameters utilized in AGE2EDOT are from *Hames and Bowring* [1994] for MAr data, *Reiners et al.* [2004] for ZHe data, and *Ketcham et al.* [1999] for AFT data. For the range of input model parameters tested, the closure temperatures for our MAr, ZHe, and AFT ages typically varied between 325°C and 400°C, 160–195°C, and 100–130°C, respectively (Table S5).

[29] Estimates for the peak temperature range and timing constraints for achieving peak temperature for GH, LH, and TH rocks in eastern Bhutan were also incorporated from *Daniel et al.* [2003], *Long et al.* [2011c], *Kellett et al.* [2010], *Whynot et al.* [2010], and *Chambers et al.* [2011] and from the thermochronologic data presented in this

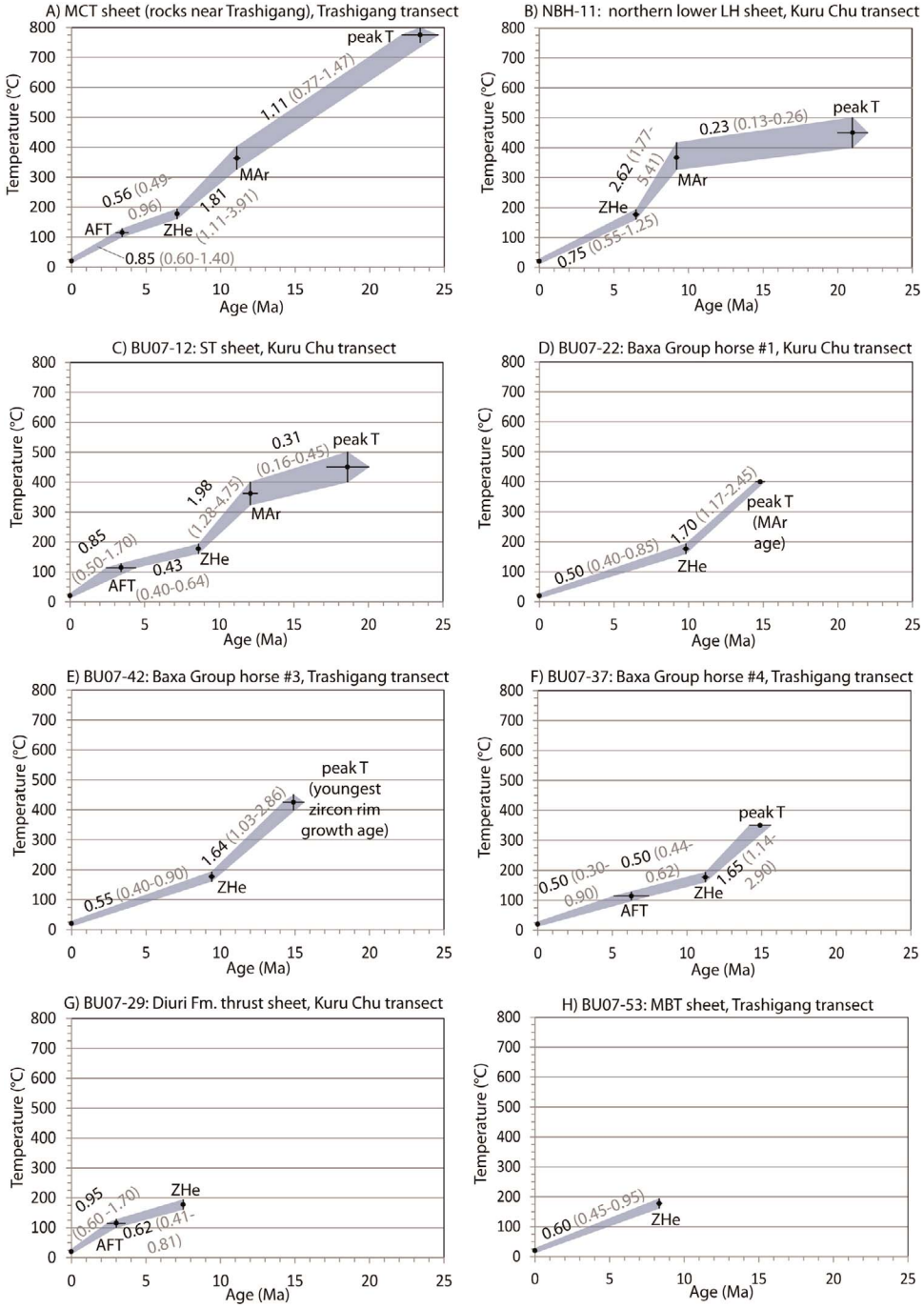

Figure 7. Temperature-time (T-t) paths for representative samples from structural systems in the Kuru Chu and Trashigang transects (see Figure S2 for T-t paths of all samples and Table S5 for supporting data). The blue swath illustrates variability between successive T-t data points, and accounts for ranges of peak temperature, ranges of closure temperature, and cooling age uncertainty. Black numbers indicate exhumation rates (mm/yr) for a 30°C/km geothermal gradient, and gray numbers indicate the permissible range of exhumation rates for given age uncertainties, closure temperature ranges, and modeled geothermal gradients (20 and 40°C/km).

study (Table S5). For each T-t path, exhumation rates were calculated that incorporate the age that the sample reached peak temperature, the age and temperature of each thermochronologic system, and the modern day surface conditions (20°C at 0 Ma) using AGE2EDOT modeling results. The AGE2EDOT results produced a range of permissible closure temperature depths and associated exhumation rates by taking into account both the uncertainty in the age that the sample achieved a given temperature, and the uncertainty in the initial geothermal gradient (20–40°C/ km). The blue swath in Figures 7 and S2, which shows the permissible variation in the T-t path, illustrates the range of closure temperatures and

ages. For each segment of the T-t path between successive data points, the exhumation rate (mm/yr) for a 30°C/km geothermal gradient and the center age is shown in black text. The gray text indicates the permissible range in exhumation rates for a 40°C/km geothermal gradient and the high age error bar (low exhumation rates) and a 20°C/km geothermal gradient and the low age error bar (high exhumation rates).

5.1. Main Central Thrust Sheet and Hanging Wall of the Lower South Tibetan Detachment

[30] The timing of initiation of motion on the MCT in eastern Bhutan is estimated from U-Pb monazite geochronology presented by *Chambers et al.* [2011]. This study documented prograde monazite growth in GH rocks just beneath the Sakteng (Radi) klippe on the Trashigang transect at 23.4 ± 1.2 Ma, indicating that burial and heating of GH rocks was taking place at this time [*Chambers et al.*, 2011]. Thus, 23.4 Ma records the maximum permissible timing for the initiation of exhumation of GH rocks. In addition, monazite crystallization at circa 21–23 Ma in schist just above the MCT west of Trashigang and circa 18–16 Ma in deformed leucogranite and migmatite 2 km above the MCT south of Trashigang suggests that crystallization of partial melts and internal, top-to-south shearing within GH rocks continued over this time period [*Daniel et al.*, 2003].

[31] The timing of motion on the STDl comes from U(-Th)-Pb monazite geochronology and U-Pb zircon geochronology [*Kellett et al.*, 2009, 2010; *Chambers et al.*, 2011]. Prograde monazite growth initiated in the Chekha Formation of the Sakteng (Radi) klippe at 21.6 ± 0.6 Ma [*Chambers et al.*, 2011]. To the west in the Ura Klippe, prograde monazite grew in GH rocks between circa 26.0 and 20.3 Ma, while retrograde monazite grew in the Chekha Formation between circa 21.8 and 16.1 Ma, suggesting motion on the STDl at this time [*Kellett et al.*, 2010]. *Kellett et al.* [2009] proposed that the STDl at the Ura klippe was active until circa 15.5 Ma, based on a U-Pb SHRIMP age of magmatic zircon crystallization in a weakly deformed, late stage leucogranite dike that intruded the Chekha Formation.

[32] In summary, the geochronologic data discussed above support ductile shearing on the STDl in eastern Bhutan between circa 23 and 16 Ma, and initiation of exhumation of GH rocks in the MCT sheet after circa 23 Ma, with internal top-to-south shearing continuing until circa 18–16 Ma [*Grujic et al.*, 2002; *Daniel et al.*, 2003; *Kellett et al.*, 2009, 2010; *Chambers et al.*, 2011].

[33] Between 23 Ma and circa 11–14 Ma (published MAr ages [*Stüwe and Foster*, 2001; *Kellett et al.*, 2009]), GH rocks in the MCT sheet were exhumed from peak temperatures between 650 and 800°C [*Daniel et al.*, 2003] to 325–400°C, yielding a time-averaged exhumation rate range of 0.9–1.4 mm/yr for a 30°C geothermal gradient, and a total exhumation rate range of 0.7–2.3 mm/yr for 40°C and 20°C geothermal gradients, respectively (note that this applies to discussion of all exhumation rates in the text below) (Figure 7a). The time period of exhumation through the MAr closure temperature postdates the ~23–16 Ma period of motion of the STDl and the ~23 to ~18–16 Ma window of emplacement of the MCT sheet. Accurate evaluation of exhumation rates of GH rocks during emplacement of the MCT and STDl would require a much more detailed analysis of the age, duration and magnitude of peak pressure and temperature conditions, as well as the use of higher-temperature thermochronologic systems.

[34] GH rocks were exhumed from 325 to 400°C to 160–195°C between circa 11–12 Ma (published MAr ages [*Stüwe and Foster*, 2001; *Kellett et al.*, 2009]) and circa 6.5–7 Ma (ZHe ages), at rates of 1.4–1.8 mm/yr (total range: 1.1–3.9 mm/yr), and from 160 to 195°C to 100–130°C between circa 7–8.5 Ma and circa 4–6.5 Ma (published AFT ages [*Grujic et al.*, 2006; *Stüwe and Foster*, 2001]), at rates of 0.6–1.3 mm/yr (total range: 0.5–1.4 mm/yr). Between circa 3–6 Ma and the present, GH rocks were exhumed from 100 to 130°C to a surface temperature of 20°C (Text S1, section 6) at rates of 0.5–0.9 mm/yr (total range: 0.3–1.4 mm/yr). The MAr, ZHe, and AFT ages from GH rocks in eastern Bhutan all postdate the emplacement of the MCT and STDl, and are interpreted to represent uplift and erosion that accompanied passive translation of GH rocks during younger deformation of LH rocks further to the foreland (see discussions in sections 5 and 6).

5.2. Lower Lesser Himalayan Duplex

[35] *Daniel et al.* [2003] obtained U-Pb ages on two metamorphic monazite grains, a precisely dated grain at 20.0 ± 0.2 Ma, and a grain that was circa 18 Ma, from a concordant Paleoproterozoic orthogneiss body intruded into the Daling Formation within the ST sheet east of Mongar (Figure 2), which they attributed to prograde metamorphism as a result of structural burial under the MCT sheet. Thus, rocks in the northern thrust sheet of the lower LH duplex on the Kuru Chu transect must have achieved peak temperatures between circa 23.4 Ma, the maximum time for initiation of motion on the MCT [*Chambers et al.*, 2011], and circa 20 Ma, the timing of prograde metamorphism of LH rocks in the ST sheet to the south (Table S5). Between 20 and 23.4 Ma and circa 8.5–13 Ma (MAr ages), rocks in this thrust sheet were exhumed from peak temperatures of 400–500°C [*Long et al.*, 2011c] to 325–400°C, at rates of 0.2–0.25 mm/yr (total range: 0.1–0.3 mm/yr) (Figure 7b). Between circa 8.5–13 Ma and circa 6–7 Ma (ZHe ages), this thrust sheet was rapidly exhumed from 325°C to 400°C to 160–195°C, at rates of 1.3–2.6 mm/yr (total range: 0.9–6.7 mm/yr), and from circa 6–7 Ma to the present, this thrust sheet was exhumed from 165 to 195°C to 20°C, at a rate of 0.8–0.9 mm/yr (0.6–1.5 mm/yr total range) (Figure 7b).

[36] The time window that rocks in the ST sheet achieved peak temperatures can be bracketed between circa 20 Ma, the timing of prograde metamorphism of orthogneiss within the Daling Formation, attributed to burial under the MCT sheet [*Daniel et al.*, 2003], and circa 17.2 Ma, the weighted mean age of metamorphic zircon rim growth in Baxa Group rocks just below the ST, which indicates that motion on the ST sheet must have been underway by this time. Between 17.2 and 20 Ma and circa 12 Ma (MAr ages), the ST sheet was exhumed from peak temperatures of 400–510°C [*Whynot et al.*, 2010; *Long et al.*, 2011c] to 325–400°C, at rates of 0.3–0.4 mm/yr (total range: 0.2–0.8 mm/yr) (Figure 7c). Between 12 Ma and 7–10 Ma (ZHe ages), the ST sheet was rapidly exhumed from 325 to 400°C to 160–195°C, at rates of 1.5–2.0 mm/yr (total range: 0.9–4.8 mm/yr), and between 7 and 10 Ma and 3.5–5 Ma (AFT ages), exhumation rates were 0.4–0.8 mm/yr (total range: 0.4–1.1 mm/yr)

(Figure 7c). Between 3.5 and 5 Ma and the present, exhumation rates were 0.7–0.9 mm/yr (total range: 0.5–1.7 mm/yr) (Figure 7c).

5.3. Upper Lesser Himalayan Duplex

[37] Baxa Group sample BU07-42, collected directly below the ST on the Trashigang transect (Figures 2 and 3), records growth of metamorphic zircon rims centered at 17.2 ± 0.5 Ma (section 4.4), which indicates that emplacement of the ST sheet must have been underway at this time. The 14.9 ± 0.7 Ma age of the youngest three zircon rims (section 4.4) indicates the maximum permissible age for the initiation of exhumation of this sample. After 14.9 Ma, BU07-42 was exhumed from a deformation temperature range of 400–450°C [*Long et al.*, 2011c] to 160–195°C by 9.42 ± 0.17 Ma (ZHe age), corresponding to an exhumation rate of 1.6 mm/yr (total range: 1.0–2.9 mm/yr) (Figure 7e).

[38] Baxa Group sample BU07-22, from horse 1 on the Kuru Chu transect (Figures 2 and 3), exhibits quartz recrystallization microstructure characteristic of the transition between bulging and subgrain rotation recrystallization (Figure 5), which corresponds to a deformation temperature of ∼400°C [*Stipp et al.*, 2002; *Long et al.*, 2011c]. Neoblastic white mica grains are observed in pressure shadows between ductiley elongated quartz clasts in BU07-22 (Figure 5), indicating that mica growth was syndeformational with the bedding-parallel flattening strain observed in this sample, which is documented in Baxa Group rocks throughout eastern and central Bhutan [*Long et al.*, 2011c]. Flattening is interpreted to have accompanied structural burial of Baxa Group thrust sheets beneath the ST sheet, prior to thrust imbrication [*Long et al.*, 2011c]. This observation, combined with a microstructural deformation temperature that does not exceed the MAr closure temperature range, leads us to interpret the circa 15 Ma neoblastic white mica age from BU07-22 (section 4.1) as the timing of structural burial of this sample beneath the ST sheet. Between ∼15 Ma and 9.82 Ma (ZHe age), BU07-22 was exhumed from 400°C to 160–195°C, corresponding to an exhumation rate of 1.7 mm/yr (total range: 1.2–2.4 mm/yr) (Figure 7d).

[39] Since all Baxa Group horses underwent structural burial and flattening strain prior to thrust imbrication and exhumation during construction of the upper LH duplex [*Long et al.*, 2011c], the ∼15 Ma burial age from BU07-22 is applied in the 1-D modeling as both the timing of achievement of peak temperature and the maximum permissible age for initiation of exhumation for samples from all Baxa Group horses on the Kuru Chu transect (Table S5). The 14.9 ± 0.7 Ma youngest zircon rim growth age is similarly applied to samples from all Baxa Group horses on the Trashigang transect (Table S5). Baxa Group samples on both transects were exhumed from a peak temperature of ∼350°C [*Whynot et al.*, 2010] to 160–195°C between circa 15 Ma and 9.5–11.5 Ma (ZHe ages), at rates of 1.1–1.7 mm/yr (total range: 0.8–3.1 mm/yr) (Figure 7f).

[40] Between 10.5 and 11.5 Ma (ZHe ages) and 6–6.5 Ma (AFT ages), Baxa Group samples BU07-37 and BU07-35 were exhumed from 160 to 195°C to 100–130°C, at rates of 0.5 mm/yr (total range: 0.4–0.7 mm/yr), indicating a significant slowing of exhumation rates (Figure 7f). Between 6 and 6.5 Ma and the present, exhumation rates for these two samples remained at 0.5 mm/yr (total range: 0.3–0.9 mm/yr) (Figure 7f).

5.4. Diuri Formation and MBT Thrust Sheets

[41] Rocks in the Diuri Formation and Gondwana succession (MBT) thrust sheets achieved deformation temperatures of 250–310°C [*Long et al.*, 2011c]. However, the age that rocks in these thrust sheets achieved peak temperature is not constrained. The timing of peak temperature must predate the oldest thermochronologic record of exhumation, which for the Diuri Formation thrust sheet is circa 11.2 Ma (ZHe age from BU07-33), and for the MBT sheet is circa 8.3 Ma (ZHe age from BU07-54). The Diuri Formation thrust sheet was exhumed at rates of 0.5–0.6 mm/yr (total range: 0.4–0.8 mm/yr) between 7.5 and 11 Ma (ZHe ages) and 3–5.5 Ma (AFT ages), and at rates of 0.5–1.0 mm/yr (total range: 0.4–1.7 mm/yr) between 3 and 5.5 Ma and the present (Figure 7g). The MBT sheet was exhumed a rate of 0.6 mm/yr (total range: 0.5–1.0 mm/yr) between circa 8.3 Ma (ZHe age) and the present (Figure 7h).

6. Timing Constraints on Lesser Himalayan Deformation: Interpretations of Thermochronology Data

6.1. Lower Lesser Himalayan Duplex and Initiation of ST

[42] The circa 20 Ma prograde monazite growth age obtained from orthogneiss within the ST sheet (section 5.2; Figure 2) indicates that structural burial of the ST sheet under the MCT sheet was underway by this time [*Daniel et al.*, 2003]. Kinematic reconstructions of both cross sections (Figures 8b and 9b) show that emplacement of the MCT sheet and partial emplacement of the northern lower LH thrust sheet are required in order for the leading edge of the MCT sheet to reach the projected position of the sampled LH orthogneiss. Thus, we suggest that emplacement of the northern lower LH thrust sheet must have initiated by circa 20 Ma.

[43] The growth of metamorphic zircon rims in Baxa Group sample BU07-42 is interpreted as the result of structural burial, which we interpret as the initiation of motion on the ST. The weighted mean age of 17.2 ± 0.5 Ma (2σ) indicates that burial was underway at this time and the circa 15 Ma age of the youngest zircon rim growth, combined with the circa 15 Ma MAr burial age from sample BU07-22 (section 5.3), mark the maximum permissible age for the initiation of exhumation of Baxa Group rocks in the upper LH duplex (section 6.2). The period of time interpreted for construction of the lower LH duplex can be bracketed between 20 Ma (age of initial burial) and 15 Ma (initiation of exhumation in the upper LH duplex). The observation that the MCT overlaps both the ST sheet and the northern lower LH thrust sheet on the Kuru Chu transect requires that the MCT acted as the roof thrust for the lower LH duplex [*McQuarrie et al.*, 2008; *Long et al.*, 2011b], and that motion on the MCT must have been concurrent with emplacement of the northern lower LH thrust sheet. This is consistent with the ∼23 to ∼18–16 Ma estimate for MCT emplacement and ∼23–16 Ma estimate for STDl motion

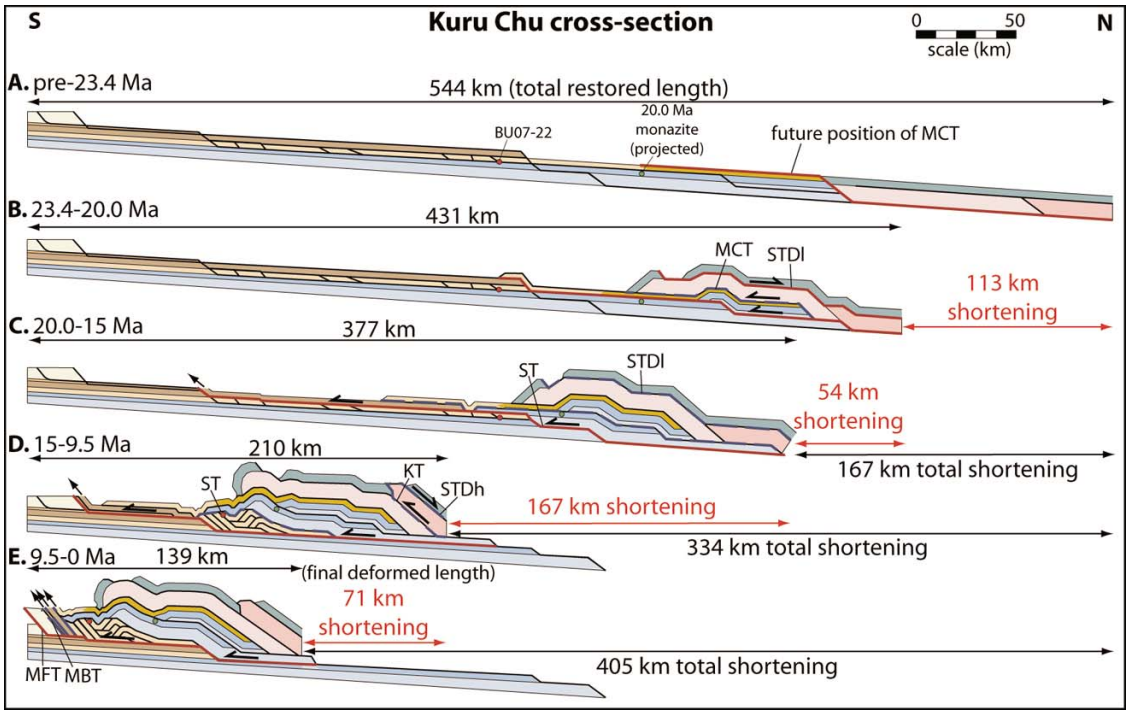

Figure 8. Sequentially restored cross sections of the Kuru Chu transect, showing deformed length, total shortening, and incremental shortening (red) accommodated in each time increment. See Table 3 for summary of timing constraints and Figure 1 caption for structure abbreviations. Solid red lines indicate structures that were active at the end of the time increment, and dashed blue lines indicate structures that were active at the beginning or at some point during the time increment but are inactive at the end. (a) Restored positions of all LH and GH thrust sheets (future position of MCT is shown). (b) Emplacement of MCT sheet and coeval top-to-north displacement on the STDl and initial emplacement of the northernmost lower LH thrust sheet. The leading edge of MCT sheet has reached the projected position of the orthogneiss sample that yielded a 20.0 ± 0.2 Ma prograde monazite age [*Daniel et al.*, 2003]. (c) Remaining construction of the lower LH duplex, including initial motion on the ST. Cross section is drafted showing the maximum amount of ST motion that took place prior to emplacement of the Baxa Group horse that contains sample BU07-22. (d) Construction of the upper LH duplex through imbrication of multiple Baxa Group horses (intraformational Baxa Group thrust faults are not outlined in blue for simplicity). (e) Emplacement of MBT and MFT sheets and passage of the upper LH duplex and the majority of the lower LH duplex over the Diuri-Baxa footwall ramp. The final deformed geometry from *Long et al.* [2011b] is shown.

summarized above [*Grujic et al.*, 2002; *Daniel et al.*, 2003; *Kellett et al.*, 2009, 2010; *Chambers et al.*, 2011].

[44] The time period of construction of the lower LH duplex is characterized by slow (0.2–0.4 mm/yr) exhumation rates, defined between initiation of deformation at 20 Ma and MAr ages of 9–13 Ma (Figures 7b, 7c, and S2). This is interpreted as the result of minimal erosion of the structurally overlying GH-TH section during this time period, possibly as a result of southward translation over a relatively flat basal detachment surface that lacked significant footwall ramps.

[45] The Mesoproterozoic (circa 1.4 Ga) MAr age from the klippe of the Daling Formation (sample BU07-21) indicates that this sample did not achieve 325–400°C temperatures during Himalayan orogenesis. This is significant because it indicates a limited amount of structural burial. We interpret that the position of this sample marks the southern limit of structural burial under the full thickness of the MCT sheet and overlying TH section, and thus that the MCT sheet did not propagate this far south.

6.2. Upper Lesser Himalayan Duplex

[46] The timing of the transition from burial to exhumation for Baxa Group horses is critical for constraining the timing for the initiation of the upper LH duplex. The circa 15 Ma weighted mean age from the 3 youngest metamorphic zircon rim ages in sample BU07-42 is interpreted as the last gasp of prograde metamorphism attributed to burial from motion on the ST. Similarly, we interpret the circa 15 Ma MAr age from sample BU07-22 as the age of burial of Baxa Group horse 1 on the Kuru Chu transect. Thus, circa 15 Ma marks the earliest possible time for the initiation of exhumation these Baxa Group samples (Figures 8c and 9c).

[47] We interpret the ZHe ages obtained from Baxa Group samples as dating the end of construction of the upper LH duplex. Exhumation from temperatures of 350–400°C (and locally as high as 400–450°C) [*Whynot et al.*, 2010; *Long et al.*, 2011c], to temperatures of 160–195°C occurred between ~15 and 10.5 Ma on the Trashigang transect (based

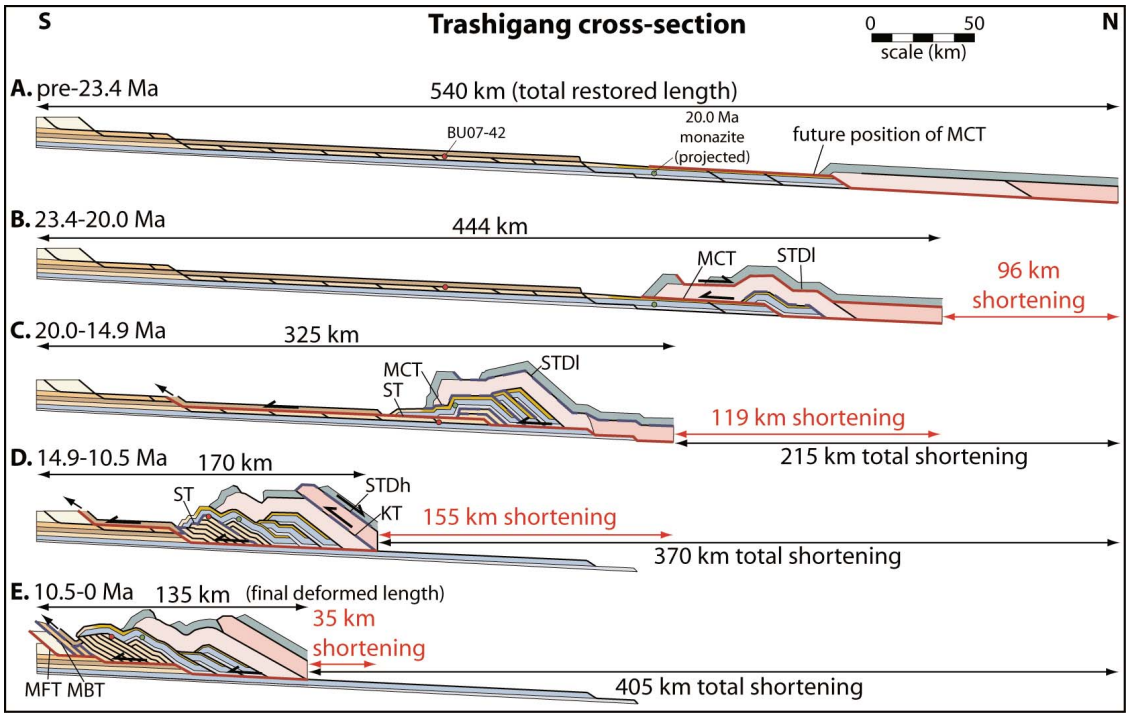

Figure 9. Sequentially restored cross sections of the Trashigang transect. Deformation increments are the same as Figure 8. See Table 3 for timing constraints and Figure 1 caption for structure abbreviations.

on the 10.5 ± 1.1 Ma weighted mean age of all five ZHe ages), and between ~15 and 9.5 Ma on the Kuru Chu transect (based on the 9.5 ± 0.6 Ma weighted mean age of all five ZHe ages). This period of rapid exhumation reached rates of 1.1–1.7 mm/yr (Figures 7d–7f). After cooling through the ZHe closure temperature range, a significant decrease in exhumation rates to 0.5 mm/yr is observed from circa 10 Ma to the present (Figures 7d–7f). This slower exhumation is interpreted as the result of passive translation during emplacement of foreland thrust sheets, including the MBT and MFT sheets (section 6.3), which postdate the majority of construction of the upper LH duplex.

6.3. Deformation in Foreland Part of Fold-Thrust Belt

[48] Quartz recrystallization microstructure from the Diuri Formation and Gondwana succession on the Trashigang transect indicate a deformation temperature range of 250°–310°C [*Long et al.*, 2011c]. This is corroborated by the Mesoproterozoic (circa 1.02–1.36 Ga) MAr age range from Diuri Formation sample BU07-29, which indicates that this sample did not achieve 325–400°C temperatures during Himalayan orogenesis. ZHe ages as young as 7.5–9 Ma from the Diuri Formation and MBT sheets indicate that cooling from 250°–310°C to 160–195°C had occurred by this time.

[49] The earliest record of exhumation in the Diuri Formation thrust sheet is the circa 11 Ma ZHe age from sample BU07-33. However, the timing of initial motion on this thrust sheet is most likely much earlier, as demonstrated in the cross-section reconstructions (Figures 8c, 8d, 9c, and 9d), which show this thrust sheet being translated over the top of the upper LH duplex as it was formed, in front of the ST sheet. Between 7.5 and 9 Ma and 3–4 Ma, exhumation rates of the Diuri Formation thrust sheet were between 0.5 and 0.6 mm/yr (Figures 7g and S2). Post 3–4 Ma exhumation rates increased to 0.5–1.0 mm/yr, and are interpreted to indicate the time that these rocks were uplifted along the MBT ramp (Figures 8e and 9e).

[50] The ~10–3 Ma age for emplacement of frontal lesser Himalayan thrust sheets is also supported by low exhumation rates in the upper LH duplex, implying translation, combined with renewed exhumation in the lower LH duplex. The period of rapid exhumation (1.3–2.6 mm/yr) between ~9–13 Ma (MAr ages) and ~4–10 Ma (ZHe ages) in the lower LH duplex is interpreted as the result of uplift, erosion and translation during the final construction of the upper LH duplex, and translation up and over a major footwall ramp through the Baxa Group and Diuri Formation during emplacement of the frontal LH thrust sheets (Figures 3, 8e, and 9e).

[51] At present, no sedimentological or thermochronologic data exist from the Siwalik Group in Bhutan to allow precise estimation of initiation of motion on the MFT. Since the MFT carries strata as young as Pliocene, some component of displacement on this structure must be circa 5 Ma or younger.

7. Kinematic History and Long-Term Crustal Shortening Rates

7.1. Incrementally Restored Balanced Cross Sections

[52] The Kuru Chu and Trashigang cross sections (Figure 3) were originally presented by *Long et al.* [2011b], along with details on geometric constraints and the methods of construction. In this study, we present sequential reconstructions of each cross section, which highlight 5 increments of deformation (Figures 8 and 9), and we quantify the

shortening magnitude between each increment. These shortening magnitudes are then combined with burial and cooling ages to place constraints on the age of motion for specific structures or groups of structures. This approach allows us to generate a four-part history of shortening rates for the Bhutan thrust belt.

[53] Figures 8a and 9a represent restoration of all LH and GH thrust sheets to their undeformed position. The total shortening of *Long et al.* [2011b] was estimated by adding the structural overlap of the MCT and KT sheets to the total restored length of LH sheets. For this sequential reconstruction, we show GH rocks as a northern continuation of the Indian margin and place the hanging wall cutoff of the MCT sheet next to the northern limit of restored LH rocks.

[54] Figures 8b and 9b illustrate south directed emplacement of the MCT sheet over lower LH rocks, and coeval top-to-the-north displacement of TH rocks along the STDl between ~23.4 and 20 Ma. In order to bury the LH orthogneiss sampled from the ST sheet at 20 Ma [*Daniel et al.*, 2003], 13 km of motion on the northernmost LH horse in both cross sections is necessary. Emplacement of the MCT sheet and initial construction of the lower LH duplex resulted in 113 km and 96 km shortening on the Kuru Chu and Trashigang transects, respectively.

[55] Figures 8c and 9c illustrate deformation between circa 20 Ma and 15 Ma, which includes the majority of construction of the lower LH duplex. Because the MCT acted as the roof thrust of the lower LH duplex [*McQuarrie et al.*, 2008; *Long et al.*, 2011b], the frontal portion of the MCT must have remained active during the completion of emplacement of northern lower LH thrust sheets. Available timing constraints suggest top-to-the-north motion on the STDl over the time window of both MCT and lower LH duplex displacement [e.g., *Grujic et al.*, 2002; *Kellett et al.*, 2009]. Thus, we schematically show a component of top-to-the-north offset on the STDl. In addition to construction of the lower LH duplex, we show enough displacement on the ST to bury samples BU07-42 on the Trashigang transect and BU07-22 on the Kuru Chu transect in increment C. Figures 8c and 9c illustrate the maximum amount of motion on the ST that occurred prior to the initiation of exhumation of samples BU07-42 and BU07-22. The shortening magnitudes for this increment are 54 km on the Kuru Chu transect and 119 km on the Trashigang transect.

[56] Figures 8d and 9d illustrate the imbrication of multiple Baxa Group horses in the construction of the upper LH duplex between ~15–9.5 Ma (Kuru Chu) and ~15–10.5 Ma (Trashigang). Klippen of the Daling Formation preserved in the southern part of the Kuru Chu transect require that the ST sheet, which acted as the roof thrust for the upper LH duplex, extended at least as far south as the southern limit of Baxa Group horses [*Long et al.*, 2011b]. Construction of the upper LH duplex accommodated the highest shortening magnitudes of any increment, with 167 km shortening on the Kuru Chu transect and 155 km shortening on the Trashigang transect.

[57] Figures 8d and 9d also show coeval top-to-the-south motion on the KT and top-to-the-north motion on the STDh in the hinterland. Circa 14–15 Ma U-Pb monazite and xenotime crystallization ages from a deformed leucogranite dike that intrudes the KT zone north of Trashigang provide a maximum age for motion on the KT [*Grujic et al.*, 2002; *Daniel et al.*, 2003]. The STDh was active until at least circa 11.0 Ma, based on a U-Pb SHRIMP zircon crystallization age from a weakly deformed (late stage) leucogranite dike emplaced in GH gneisses ~1 km below this structure in northwest Bhutan [*Kellett et al.*, 2009]. It has been postulated that the KT and STDh were concurrently active, in a similar manner to the MCT-STDl system [*Grujic et al.*, 2002; *Kellett et al.*, 2009]. In this study, we follow this postulation, and in our reconstructions we show coeval shearing on the KT-STDh system between circa 15 and 11 Ma, based on the timing constraints discussed above. This motion timing range is also supported by the results of recent studies in the hanging wall of the Laya thrust in northwest Bhutan (Figure 1), which is interpreted as the western continuation of the KT [*Grujic et al.*, 2011; *Warren et al.*, 2011, 2012]. On Figures 8d and 9d, the KT is shown cutting the STDl, after the interpretation of *Kellett et al.* [2009], and has 31 km (Kuru Chu) to 42 km (Trashigang) of displacement [*Long et al.*, 2011b]. The STDh is schematically shown with a small amount (~15 km) of offset.

[58] Figures 8e and 9e show the final deformed geometry of each cross section [*Long et al.*, 2011b]. Between cross sections in Figures 8d and 9d and 8e and 9e, during emplacement of the MBT and MFT sheets, the entire upper LH duplex, the majority of the lower LH duplex, and much of the MCT sheet were translated up and over a major subsurface footwall ramp through the Baxa Group and Diuri Formation [*Long et al.*, 2011b]. This translation accommodated 71 km of shortening on the Kuru Chu transect and 35 km on the Trashigang transect.

7.2. Discussion of Constraints on Balanced Cross Sections

[59] The cross sections are constrained by 1:50,000-scale geologic mapping [*Long et al.*, 2011b], tectonostratigraphy of SH, LH, and GH rocks [*Long and McQuarrie*, 2010; *Long et al.*, 2011a, 2011b], and a general 4°N northward dip of the basement-cover contact [*Ni and Barazangi*, 1984; *Hauck et al.*, 1998; *Pandey et al.*, 1999; *Mitra et al.*, 2005]. The positions of hanging wall cutoffs of thrust sheets, where unconstrained, were drafted just above the erosion surface, in order to minimize structural overlap. The following paragraphs summarize important constraints on deformation geometries, from foreland to hinterland.

[60] 1. For the MFT sheet, a lack of repetition of the three-part Siwalik Group stratigraphy indicates the presence of only one thrust sheet. The hanging wall cutoff of the MFT sheet has passed through the erosion surface, so displacement shown on the MFT is a minimum. However, since the subsurface position of the footwall ramp through the Baxa Group and Diuri Formation is well constrained (see discussion below), lengthening of the MFT sheet would be balanced by a comparable decrease in length of the MBT (Gondwana succession) thrust sheet, thus resulting in similar overall shortening.

[61] 2. For the MBT sheet, the hanging wall cutoff for the MBT sheet has also passed through the erosion surface; however, the restored length of the Gondwana succession must correspond to the length of the Diuri Formation between the Gondwana succession footwall ramp and the Diuri Formation-Baxa Group footwall ramp. The latter ramp is well constrained on the Kuru Chu cross section by a

significant steepening of dips in the Daling-Shumar Group (Figure 3a). On the Trashigang cross section, this footwall ramp could be positioned further to the north, but this would decrease the restored length of Daling-Shumar Group horses, and add a comparable length to the restored Baxa Group-Diuri Formation section, thereby keeping overall shortening approximately the same.

[62] 3. For the Diuri Formation thrust sheet, the Diuri Formation is observed in stratigraphic contact over the Baxa Group in 2 localities in the southern part of the Kuru Chu transect (Figure 2). This indicates that the length of the Diuri Formation thrust sheet must equal the total restored length of duplexed Baxa Group horses, and therefore that the majority of the original length of the Diuri Formation thrust sheet was displaced to the south and eroded as the upper LH duplex grew. Adding additional length to this thrust sheet would necessitate adding an equivalent length of additional Baxa Group horses between the surface and the décollemont. The cross sections that we show here fill that entire space with repeated Baxa Group horses, limiting additional shortening of the Baxa Group.

[63] 4. For the upper LH duplex, the thickness of repeated Baxa Group horses is constrained by lower thrust contacts and upper stratigraphic contacts with the Diuri Formation observed in two thrust sheets on the southern Kuru Chu transect, and the spacing of localized zones of deformation interpreted as the sites of intraformational thrust faults further north on the Kuru Chu transect and on the Trashigang transect. Klippe of the Daling Formation observed on the Kuru Chu transect require that the ST sheet extends over all exposed Baxa Group horses, and limits the length of the leading edge of Baxa Group horses to ~2–3 km above the modern erosion surface.

[64] 5. For the lower LH duplex, the hanging wall ramp through the Shumar Formation in the ST sheet is observed on both the Kuru Chu and Trashigang transects. The thickness of repeated lower LH thrust sheets is constrained by repetition of the two-part stratigraphy of the Daling-Shumar Group on the Kuru Chu transect. Regional-scale, long-wavelength, low-amplitude, E-W trending folds in the MCT sheet are interpreted as the result of duplexing of lower LH thrust sheets at depth.

[65] 6. For the MCT thrust sheet, the hanging wall cutoff for the MCT sheet has passed through erosion surface; however, the Proterozoic MAr age from Daling klippe sample BU07-21 indicates a lack of heating above ~350–400°C (Figure 2 and Table 1). We interpret that the position of this sample marks the southern permissible limit of structural burial under the full thickness of the MCT sheet and overlying TH section and thus that the MCT sheet did not propagate this far south.

[66] 7. For the KT thrust sheet, the hanging wall cutoff for the KT sheet has also passed through the erosion surface. The amount of displacement on the KT sheet is one of the largest unknowns on the balanced cross sections.

[67] 8. For internal strain, in our reconstructions, we treated all thrust sheets as rigid bodies that were translated by discrete structures and did not undergo any internal strain. *Long et al.* [2011c] documented that the MCT sheet, Baxa Group horses, and Diuri Formation thrust sheet underwent layer-normal flattening strain, with approximately equal N-S and E-W elongations. This pure shear dominated strain was interpreted as the result of thrust sheet loading accompanied by volume loss, which predated thrust imbrication [*Long et al.*, 2011c; also see *Corrie et al.*, 2012]. Therefore, restoration of this layer-normal flattening strain would not result in a net increase in the original length of thrust sheets. This contrasts with the common conception that not accounting for internal strain results in underestimation of overall shortening in balanced cross sections, such as in orogenic belts that contain thrust sheets dominated by layer-parallel shortening strain [e.g., *Mitra*, 1994; *Yonkee and Weil*, 2010; *Sak et al.*, 2012].

7.3. Record of Incremental and Total Horizontal Shortening Rates

[68] We calculated shortening rates by dividing the shortening in each increment by the length of time each increment of deformation represents, with the range of shortening rates reflecting age error estimates (Figure 10 and Table 3). Initial emplacement of the MCT sheet and northern lower LH thrust sheet between circa 23.4 and 20 Ma (increment B) corresponds to rates of 33 mm/yr (24–57 mm/yr range) on the Kuru Chu transect and 28 mm/yr (20–48 mm/yr range) on the Trashigang transect. Construction of the lower LH duplex and initial emplacement of the ST sheet between circa 20 and 15 Ma (increment C) corresponds to rates of 10 mm/yr (9.4–12 mm/yr range) on the Kuru Chu transect and 23 mm/yr (20–28 mm/yr range) on the Trashigang transect. Construction of the upper LH duplex between circa 15 Ma and 9.5–10.5 Ma (increment D) corresponds to 32 mm/yr (27–39 mm/yr range) rates on the Kuru Chu transect and 35 mm/yr (25–60 mm/yr range) rates on the Trashigang transect. Finally, emplacement of foreland thrust sheets, including the MBT and MFT sheets, between circa 9.5–10.5 and 0 Ma, corresponds to rates of 7.5 mm/yr (7–8 mm/yr range) on the Kuru Chu transect and 3.3 mm/yr (3.0–3.7 mm/yr range) on the Trashigang transect.

[69] One additional incremental shortening rate is shown on Figure 10a, and it is calculated from the south-to-north younging trend observed in the seven ZHe dates from lower LH sheets on the Kuru Chu transect, and four ZHe dates from the GH section that fall on or close to the Kuru Chu section line (Figures 2 and 11). We interpret the rapid cooling of these samples through the ZHe closure temperature (Figures 7b and 7c) as the result of erosion initiated by a vertical component of motion over a footwall ramp (Figures 3a, 8d, and 8e). Thus, a graph of age versus distance would indicate the time-averaged rate of translation on the Main Himalayan thrust (MHT) over that time. Figure 11 shows a graph of these 11 ZHe ages versus map distance south of the northernmost sample (BH-378). The uniform age trend with distance defines a horizontal motion rate of 9.6 $\pm$ 0.2 mm/yr between circa 4 and 10 Ma. This age trend is interpreted as the result of exhumation and cooling associated with translation of the lower LH thrust sheets and the MCT sheet over a subsurface footwall ramp through the Baxa Group and Diuri Formation (Figures 3a, 8d, and 8e). This motion rate is similar to, but 2–3 mm/yr faster than, the 7–8 mm/yr rate estimated between 9.5 and 0 Ma for emplacement of foreland thrust sheets on the Kuru Chu transect (Figure 10a).

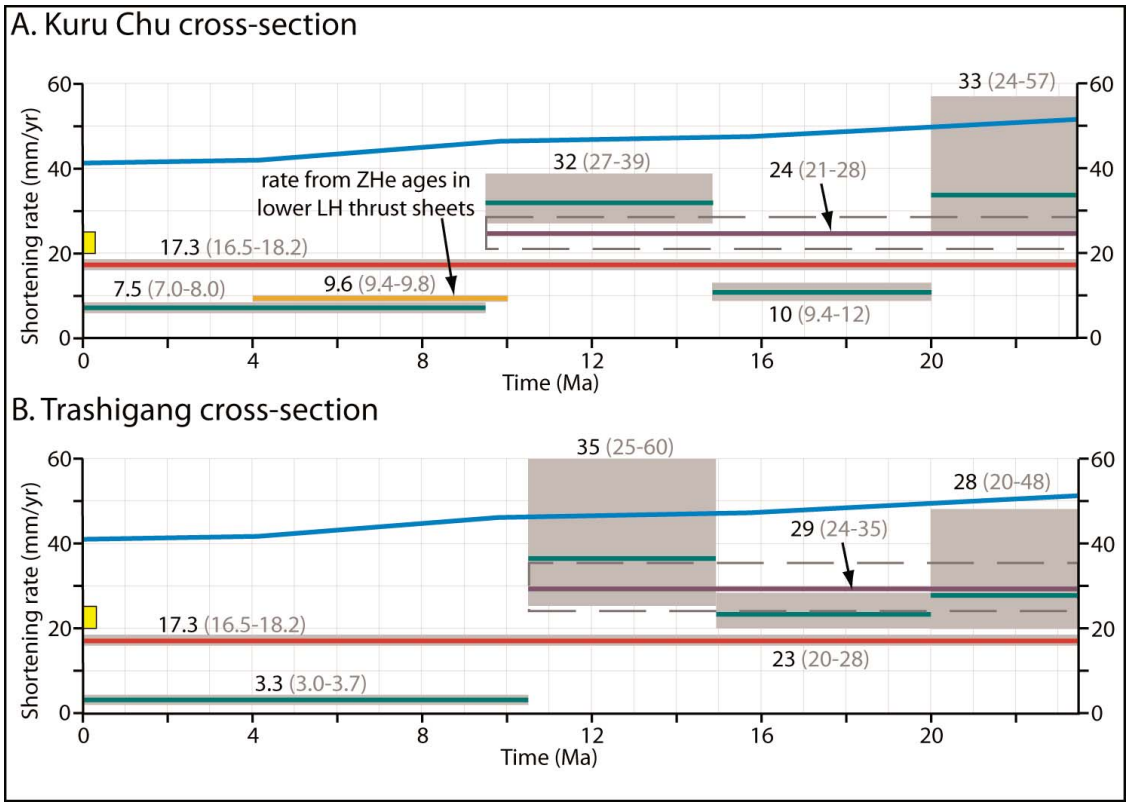

Figure 10. Graphs of horizontal shortening rate versus time, showing age trends in shortening rates accommodated by the Bhutan fold-thrust belt for (a) the Kuru Chu cross section and (b) the Trashigang cross section. See Table 3 for timing constraints and a list of shortening rates. The blue line shows overall India-Asia convergence rate [from *Copley et al.*, 2010]. The yellow box shows range of GPS convergence rates for the eastern Himalayan thrust belt (~20–25 mm/yr [*Banerjee et al.*, 2008]). The green lines are data from this study and show shortening rates for the increments of deformation in Figures 8 and 9, and the gray boxes show corresponding upper and lower error bounds. The red line shows the long-term average shortening rate between 23.4 and 0 Ma from our data (17.3 mm/yr for both transects). The orange line (only on Figure 10a) shows the horizontal motion rate calculated from the ZHe age trend in lower LH thrust sheets on the Kuru Chu transect (Figure 11). The purple line shows the faster long-term shortening rate between ~23 and 10 Ma, and dashed lines show corresponding upper and lower error bounds.

Table 3. Shortening and Shortening Rate Data for All Deformation Increments

Deformation Increment	Deformed Length (km)	Incremental Shortening (km)	Total Shortening (km)	Time Range (Ma)	Shortening Rate (mm/yr)	Shortening Rate Error Range (mm/yr)
			Kuru Chu Cross Section			
A	544	0	0	pre-23.4 ± 1.2[a]	-	-
B	431	113	113	23.4 ± 1.2[a] to 20.0 ± 0.2[b]	33.2	23.5–56.5
C	377	54	167	20.0 ± 0.2[b] to 14.78 ± 0.34[c]	10.3	9.4–11.5
D	210	167	334	14.78 ± 0.34[c] to 9.5 ± 0.6[d]	31.6	26.8–38.5
E	139	71	405	9.5 ± 0.6[d] to 0	7.5	7.0–8.0
			Trashigang Cross Section			
A	540	0	0	pre-23.4 ± 1.2[a]	-	-
B	444	96	96	23.4 ± 1.2[a] to 20.0 ± 0.2[b]	28.2	20.0–48.0
C	325	119	215	20.0 ± 0.2[b] to 14.9 ± 0.7[e]	23.3	19.8–28.3
D	170	155	370	14.9 ± 0.7[e] to 10.5 ± 1.1[f]	35.2	25.0–59.6
E	135	35	405	10.5 ± 1.1[f] to 0	3.3	3.0–3.7

[a]Data source for timing constraints *Chambers et al.* [2011].
[b]Data source for timing constraints *Daniel et al.* [2003].
[c]MAr burial age from BU07-22.
[d]Weighted mean age (95% confidence) of five Baxa Group ZHe ages on Kuru Chu transect.
[e]Youngest U-Pb zircon rim growth age from BU07-42.
[f]Weighted mean age (95% confidence) of five Baxa Group ZHe ages on Trashigang transect.

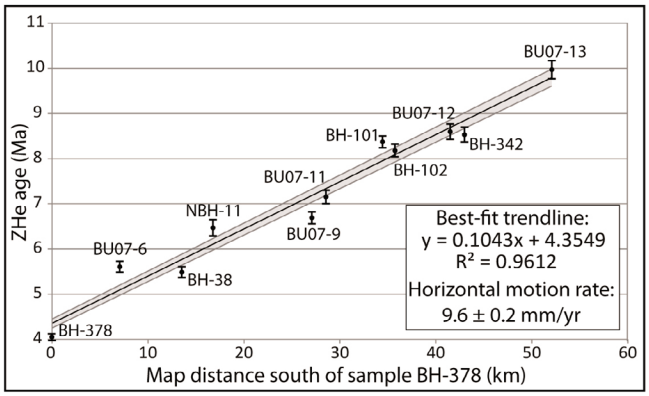

Figure 11. Graph of ZHe ages in lower LH thrust sheets and the MCT sheet on the Kuru Chu transect versus map distance (km) south of the northernmost sample (BH-378). The age trend is interpreted as exhumation and cooling associated with translation over a subsurface footwall ramp through the Baxa Group and Diuri Formation (Figure 3a). The best fit trend line defines a horizontal motion rate of 9.6 ± 0.2 mm/yr between ~10 and 4 Ma. This motion rate is plotted on Figure 10a.

[70] The total long-term rate for all shortening accommodated in the Bhutan thrust belt, which is calculated from 405 km of shortening between 23.4 Ma and the present, is 17.3 mm/yr (16.5–18.2 mm/yr range) for both cross sections (Figure 10).

8. Discussion: Implications of the Record of Shortening Rates in the Bhutan Thrust Belt

8.1. Comparison of Bhutan Shortening Rates With Published Rates of Shortening and Convergence

[71] GPS convergence rates across the western and central Himalayan thrust belt range between ~15 and 20 mm/yr [*Bilham et al.*, 1997; *Larson et al.*, 1999; *Lavé and Avouac*, 2000; *Banerjee and Burgmann*, 2002; *Zhang et al.*, 2004] and increase to ~20–25 mm/yr across the eastern Himalayan thrust belt [*Banerjee et al.*, 2008]. These rates are similar to the 21 ± 1.5 mm/yr and 19 ± 5 mm/yr Holocene shortening rates obtained in western Nepal [*Lavé and Avouac*, 2000; *Mugnier et al.*, 2004], and are also similar to the estimated 19 ± 5 mm/yr rate of southward pinch-out migration of Middle Miocene (~13–15 Ma) and younger strata in the Himalayan foreland basin [*Mugnier and Huyghe*, 2006]. Balanced cross sections across the Himalayan orogen [*DeCelles et al.*, 2002; *Long et al.*, 2011b] show that between about 400 and 670 km of total shortening has been accommodated by deformation of SH, LH, and GH rocks in the last circa 23–25 Ma, indicating long-term shortening rates between ~16 and 29 mm/yr. The overlap between the long-term, Holocene, and GPS rates has led to the prevailing assumption that the shortening rate along the basal décollement of the thrust belt (the MHT) has been constant through time [e.g., *Herman et al.*, 2010].

[72] In contrast, the four-part record of shortening rates that we obtain in this study indicates significant temporal variability. We estimate a 17.3 mm/yr long-term shortening rate for all shortening in the Bhutan thrust belt accommodated between ~23 and 0 Ma, which is similar to, but slightly slower than, the ~20–25 mm/yr GPS convergence rates measured across the eastern Himalayan thrust belt [*Banerjee et al.*, 2008]. However, we document periods of fast deformation between 23 and 20 Ma (28–33 mm/yr) and 15–10 Ma (32–35 mm/yr) that are significantly faster than the long-term average. In addition, we document a period of slower deformation between 20 and 15 Ma (10–23 mm/yr), with rates similar to, or slower than, the long-term rate, and a period of very slow deformation from 10 to 0 Ma (3–10 mm/yr). The markedly slow rate from 10 to 0 Ma skews the 23–0 Ma shortening rate to a lower value, perhaps hindering a representative comparison with modern convergence rates. Instead, a more representative measure of the long-term shortening rates accommodated by the Bhutan thrust belt may be to examine shortening rates between ~23 and 10 Ma, which are 24 mm/yr (21–28 mm/yr range) for the Kuru Chu transect and 29 mm/yr (total range 24–35 mm/yr) for the Trashigang transect (Figure 10). These rates are similar to the ~20–25 mm/yr GPS rates measured across the eastern Himalayan thrust belt [*Banerjee et al.*, 2008], but both are dramatically different than the shortening rates calculated for the last 10 Myr.

[73] Within the limits of estimated error, shortening rates approached tectonic velocities during emplacement of the MCT sheet between 23 and 20 Ma on both transects (Figure 10) and during construction of the upper LH duplex on the Trashigang transect between 15 and 10 Ma (Figure 10b). Thus, for periods of time between 23 and 20 Ma and 15–10 Ma, the Bhutan thrust belt may have absorbed nearly all India-Asian convergence at this longitude. Thrusting at tectonic velocity has also been proposed at ~10 Ma for the Ramgarh thrust in central Nepal [*Kohn et al.*, 2004], which is interpreted as a correlative structure to the ST [*Long et al.*, 2011b], and for the MCT in western Bhutan between ~20 and 15 Ma [*Tobgay et al.*, 2012].

8.2. Implications for the Timing and Relative Magnitudes of Strain Partitioning Between the Bhutan Thrust Belt and the Greater Himalayan-Tibetan Orogen

[74] The most significant change in shortening rates occurs at ~10 Ma, with a decrease to 7–10 mm/yr on the Kuru Chu transect, and 3–4 mm/yr on the Trashigang transect (Figure 10). A graph of total percent shortening versus time for each transect (Figure 12) shows that 82% (Kuru Chu) to 91% (Trashigang) of the total shortening in the Bhutan thrust belt had been accommodated between 23 and 10 Ma, leaving only 9–18% between 10 and 0 Ma. Since the hanging wall cutoffs of the MFT and MBT sheets have passed through the erosion surface, and since the hanging wall cutoff of the MFT sheet was drafted just above the erosion surface to minimize shortening (Figure 3), the 3–10 mm/yr shortening rates estimated between 10 and 0 Ma may represent minima [*Long et al.*, 2011b]. However, for the cross section to be balanced, the maximum length of the MBT sheet controls the position of the subsurface footwall ramp through the Baxa Group and Diuri Formation (Figure 3) [*Long et al.*, 2011b]. Thus, additional shortening accommodated by slip on the MFT (i.e., lengthening of the Siwalik Group thrust sheet on the restored sections) or increased shortening on the

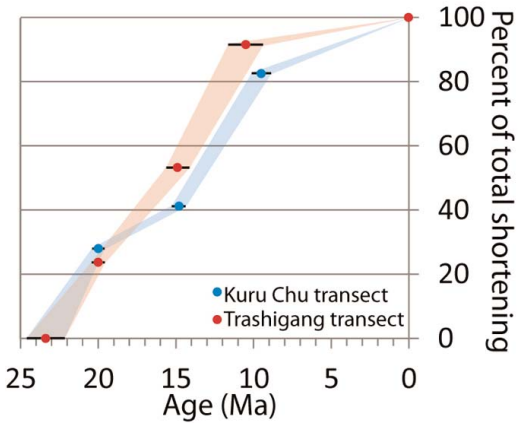

Figure 12. Graph of the percent of the total 405 km shortening on each cross section versus time. Blue and red swaths show the range of total percent shortening values based on age errors between deformation increments (Table 3) on the Kuru Chu and Trashigang transects, respectively. On the Kuru Chu transect, 82% of total shortening had been accommodated by ~9.5 Ma, and on the Trashigang transect, 91% of total shortening had been accommodated by ~10.5 Ma.

MBT would require a change in the location of this footwall ramp. However, the location of the ramp is constrained by the change from flat to steeply northward dipping bedding in the northern Kuru Chu valley (Figure 3a). The translation of rocks up and over this ramp in the last 10 Myr is supported by the younging trend in ZHe ages observed in lower LH rocks on the Kuru Chu transect between 10 and 4 Ma (Figure 11), which defines a 9.6 mm/yr horizontal motion rate. This rate should be similar to the rate of shortening during emplacement of foreland thrust sheets, which is estimated at 7–8 mm/yr between 9.5 and 0 Ma (Figure 10a).

[75] We interpret the decrease in shortening rates in the Bhutan thrust belt at ~10 Ma to represent the onset of partitioning of India-Asia convergence in the eastern part of the greater Himalayan-Tibetan orogenic system. This can in part be attributed to uplift of the Shillong Plateau, a pop-up structure bound by high-angle reverse faults that deform Indian crystalline basement [e.g., *Bilham and England*, 2001; *Biswas et al.*, 2007; *Clark and Bilham*, 2008], located 100–200 km south of Bhutan. Based on low-temperature thermochronometry, *Clark and Bilham* [2008] interpreted that uplift of the plateau initiated sometime between 8 and 14 Ma. *Biswas et al.* [2007], using multiple low-temperature thermochronometers on basement rocks exposed in the plateau, concluded that exhumation began by at least 9–15 Ma, although they state that since their thermochronometers only capture the latest portion of the total cooling history, exhumation could have started earlier. These uplift timing ranges are consistent with the circa 10 Ma decrease in shortening rates that we observe in the Bhutan thrust belt.

[76] The long-term horizontal shortening rate accommodated by uplift of the Shillong Plateau has been estimated in several studies. *Bilham and England* [2001], using geometric reconstructions of faults bounding the plateau, estimated a shortening rate of 2–6 mm/yr. However, this estimate is based on the assumption that plateau uplift started between circa 2 and 5 Ma. *Biswas et al.* [2007] presented a refined estimate of 0.65–2.3 mm/yr, by using the same reconstructions as *Bilham and England* [2001], combined with their thermochronologic exhumation rates. *Clark and Bilham* [2008], also using thermochronologic exhumation rates combined with geometric reconstructions, estimated a shortening rate of 1–3 mm/yr.

[77] Assuming that the ~24–29 mm/yr long-term shortening rate that we estimate for the Bhutan thrust belt between 23 and 10 Ma is equal to the convergence rate that was partitioned between the Bhutan thrust belt and the Shillong Plateau between 10 and 0 Ma, the 0.65–3 mm/yr shortening rate estimates for the plateau [*Biswas et al.*, 2007; *Clark and Bilham*, 2008] only account for ~2–13% of the total, and our 3–4 mm/yr (Trashigang) and 7–10 mm/yr (Kuru Chu) shortening rates estimated for the Bhutan thrust belt only account for ~11–42% of the total. Thus, strain partitioning between the Bhutan thrust belt and Shillong Plateau alone was insufficient to account for all Himalayan convergence. If we were to assume that the long-term shortening rate of ~17 mm/yr that we estimate for all Bhutan shortening between 23 and 0 Ma is more representative, the total shortening accommodated in the thrust belt and the plateau from 10 to 0 Ma (~4–13 mm/yr) would only represent 25–75% of the long-term average.

[78] We propose that the remaining convergence was accommodated by deformation in the Tibetan Plateau. The Middle and early Late Miocene (circa 13–8 Ma) was a time of plateauwide structural reorganization of deformation, including the initiation of contractional deformation and outward growth of the northern and eastern parts of the plateau [e.g., *Lease et al.*, 2011]. Evidence for this includes the onset of E-W extension in the plateau interior at circa 14–8 Ma [*Blisniuk et al.*, 2001], expansion of the SE margin of the plateau after circa 13–11 Ma [*Clark et al.*, 2005], and the onset of widespread contractional deformation in the NE part of the plateau at circa 13 Ma [*Lease et al.*, 2011], between circa 10 and 7 Ma [*Craddock et al.*, 2011], and at circa 8 Ma [*Zheng et al.*, 2006].

[79] GPS motion rates indicate that sites in southern Tibet, just north of the Bhutan thrust belt, are moving southward relative to stable India at 25–30 mm/yr, and that sites on the Shillong Plateau are moving southward relative to stable India at 4–7 mm/yr [*Banerjee et al.*, 2008]. Thus, modern convergence rates across the Bhutan thrust belt are ~20–25 mm/yr [*Banerjee et al.*, 2008]. These rates are ~15–20 mm/yr faster than the long-term shortening rates that we estimate for the Bhutan thrust belt between ~10 Ma and the present, and more than double the ~0.7–3.0 mm/yr long-term rates estimated for the Shillong Plateau between ~8–15 Ma and the present [*Biswas et al.*, 2007; *Clark and Bilham*, 2008]. This difference argues for a geologically recent acceleration of convergence rates in both the Shillong Plateau [*Banerjee et al.*, 2008] and the eastern Himalayan thrust belt. The age trend of ZHe data from lower LH rocks on the Kuru Chu transect (Figure 11) suggests a 9.6 mm/yr horizontal motion rate on the MHT between ~10 and 4 Ma, which implies that this shortening rate acceleration occurred within the last 4 Myr. However, we cannot more precisely date this event with the resolution of the techniques that we utilize. This topic could be addressed with future structural, geomorphic, stratigraphic, and/or thermochronologic

analysis of the frontal part of the eastern Himalayan thrust belt, including the MBT and MFT sheets, and the structures bounding the Shillong Plateau.

8.3. Implications of the Overlap in Timing of LH Duplexing and the KT-STDh System

[80] The circa 15–11 Ma timing range estimated for coeval motion on the KT-STDh system [*Grujic et al.*, 2002; 2011; *Daniel et al.*, 2003; *Kellett et al.*, 2009; *Warren et al.*, 2011, 2012] coincides with the circa 15–10 Ma construction of the upper LH duplex, which involved a 160–170 km forward propagation of the thrust front. Motion on the KT-STDh system could represent deformation within the internal part of the fold-thrust belt that acted as a taper-building mechanism that helped drive forward propagation and imbrication of Baxa Group thrust sheets [e.g., *Chapple*, 1978; *Davis et al.*, 1983; *Platt*, 1986; *DeCelles*, 1994]. The taper-reducing effect of frontal imbrication of multiple Baxa Group horses may have been offset by the taper-increasing effect of out-of-sequence motion on the KT in the hinterland.

[81] Though the KT-STDh system has been interpreted as a ductile crustal channel emplaced by gravity-driven southward extrusion [*Grujic et al.*, 2002; *Hollister and Grujic*, 2006], we argue that this out-of-sequence hinterland deformation could represent a taper-building mechanism regardless of the specific emplacement mechanism (for example, end-member models could range from a ductilely deformed thrust sheet with a discrete basal bounding shear zone, to more distributed deformation with the kinematics of a channel). This suggests that the driving mechanism for KT motion would be the restoration of taper to promote forward propagation of the thrust belt, with enhanced erosion being a function of the resulting increase in topography. Thus, channel flow may act as a passive response of orogen wedge taper dynamics.

9. Conclusions

[82] 1. New and published MAr, ZHe, AFT, and U-Pb (zircon) ages from LH, GH, and TH rocks in eastern Bhutan, combined with published estimates of peak temperature and ages of prograde metamorphism in GH and LH rocks, illustrate a general N to S temporal progression of Himalayan deformation between 23 and 0 Ma. The MCT sheet was emplaced between ~23 and 16 Ma, the lower LH duplex was constructed between ~20 and 15 Ma, the upper LH duplex was constructed between ~15 and 10 Ma, and foreland thrust sheets, including the MBT and MFT sheets, were emplaced between ~10 and 0 Ma.

[83] 2. Thrust sheets in the lower LH duplex were exhumed from peak temperatures of 400–500°C at ~20 Ma, through 325–400°C between 8 and 13 Ma (MAr ages), through 160–195°C between 6 and 10 Ma (ZHe ages), and through 100–130°C between 3 and 5 Ma (AFT ages). These cooling ages postdate the ~15–20 Ma construction of the duplex, and are associated with passive transport, uplift and erosion during younger deformation of upper LH rocks further to the foreland, and translation over a footwall ramp. Exhumation rates for lower LH rocks were as high as 1.3–2.6 mm/yr, and slowed to 0.4–0.9 mm/yr after passing over the footwall ramp.

[84] 3. Baxa Group thrust sheets in the upper LH duplex were buried to peak temperatures of 350–450°C at ~15 Ma, based on an MAr burial age recording syndeformational mica growth, and the age of youngest U-Pb zircon rim growth in Baxa Group samples. Baxa Group thrust sheets were exhumed through 160–195°C between 11.5 and 8.5 Ma (ZHe ages), and through 100–130°C at 6 Ma (AFT ages). Exhumation rates were between 1.1 and 1.7 mm/yr between ~15 and 10 Ma, and afterward slowed to 0.5 mm/yr.

[85] 4. Foreland LH thrust sheets, including the Diuri Formation and MBT sheets, were exhumed from peak temperatures of 250–310°C, through 160–195°C between 9 and 7.5 Ma (ZHe ages), and through 100–130°C between 3 and 6 Ma (AFT ages). Exhumation rates for these foreland thrust sheets were between 0.5 and 0.6 mm/yr from 9 to 7.5 Ma to the present, and were as high as 1.0 mm/yr between 4 and 0 Ma.

[86] 5. The Bhutan thrust belt accommodated variable shortening rates between ~23 and 0 Ma and is characterized by rapid rates (24–29 mm/yr) between ~23 and 10 Ma, followed by a decrease to 7–10 mm/yr (and possibly as low as 3–4 mm/yr) from ~10 to 0 Ma. The decrease at ~10 Ma is interpreted as the onset of strain partitioning between shortening in the Bhutan thrust belt, uplift of the Shillong Plateau, and deformation and outward growth of the eastern and northern Tibetan Plateau.

[87] 6. Within estimated error, shortening rates during emplacement of the MCT sheet and during construction of the upper LH duplex approached India-Asia tectonic velocities. Thus, for periods of time between 23 and 20 Ma and 15–10 Ma, the Bhutan thrust belt may have absorbed nearly all India-Asian convergence at this longitude.

[88] 7. Construction of the upper LH duplex, which involved a ~170 km propagation of the thrust front, is coeval with ~15–11 Ma hinterland emplacement of the KT-STDh system. We interpret this as a taper-building mechanism that helped drive forward propagation of the thrust belt. This suggests that channel flow may act as a passive response of orogen wedge taper dynamics.

[89] **Acknowledgments.** We would like to thank the government of Bhutan for their assistance and support, particularly the late Director General D. Wangda and the current Chief Geologist/Head U. Wangda of the Department of Geology and Mines in the Ministry of Economic Affairs. We would also like to thank George Gehrels and Victor Valencia at the University of Arizona LaserChron Center, Stefan Nicolescu and Uttam Choudhary at the Arizona Radiogenic Helium Dating Laboratory, Matthew Kliffer at the Dalhousie University Fission Track Research Laboratory, and Alka Tripathy at the Arizona State University Noble Gas Geochronology and Geochemistry Laboratories for their assistance. We are also grateful to Djordje Grujic for the use of mineral separates from several samples that he collected (those with BH prefix). We would also like to thank Peter van der Beek and an anonymous reviewer for constructive reviews of this manuscript. This work was primarily funded by NSF EAR 0738522 to N. McQuarrie, and partially by NSF EAR 0838112 to K. Hodges and a Geological Society of America Graduate Student Research Grant to S. Long.

References

Banerjee, P., and R. Burgmann (2002), Convergence across the northwest Himalaya from GPS measurement, *Geophys. Res. Lett.*, *29*(13), 1652, doi:10.1029/2002GL015184.

Banerjee, P., R. Burgmann, B. Nagarajan, and E. Apel (2008), Intraplate deformation of the Indian subcontinent, *Geophys. Res. Lett.*, *35*, L18301, doi:10.1029/2008GL035468.

Bettinelli, P., J. P. Avouac, M. Flouzat, F. Jouanne, L. Bollinger, P. Willis, and G. R. Chitrakar (2006), Plate motion of India and interseismic strain

in the Nepal Himalaya from GPS and DORIS measurements, *J. Geod.*, *80*, 567–589, doi:10.1007/s00190-006-0030-3.

Bhargava, O. N. (1995), *The Bhutan Himalaya: A Geological Account*, *Spec. Publ. Ser. Geol. Surv. India*, *39*, 245 pp.

Bilham, R., and P. England (2001), Plateau 'pop-up' in the great 1897 Assam earthquake, *Nature*, *410*, 806–809, doi:10.1038/35071057.

Bilham, R., K. Larson, J. Freymueller, and Project Idylhim Members (1997), GPS measurements of present-day convergence across the Nepal Himalaya, *Nature*, *386*, 61–64, doi:10.1038/386061a0.

Biswas, S., I. Coutand, D. Grujic, C. Hager, D. Stockli, and B. Grasemann (2007), Exhumation and uplift of the Shillong plateau and its influence on the eastern Himalayas: New constraints from apatite and zircon (U-Th-[Sm])/He and apatite fission track analyses, *Tectonics*, *26*, TC6013, doi:10.1029/2007TC002125.

Blisniuk, P. M., B. R. Hacker, J. Glodny, L. Ratschbacher, S. W. Bi, Z. H. Wu, M. O. McWilliams, and A. Calvert (2001), Normal faulting in central Tibet since at least 13.5 Myr ago, *Nature*, *412*, 628–632, doi:10.1038/35088045.

Brandon, M. T., M. K. Roden-Tice, and J. I. Garver (1998), Late Cenozoic exhumation of the Cascadia accretionary wedge in the Olympic Mountains, northwest Washington State, *Geol. Soc. Am. Bull.*, *110*, 985–1009, doi:10.1130/0016-7606(1998)110<0985:LCEOTC>2.3.CO;2.

Burchfiel, B. C., C. Zhiliang, K. V. Hodges, L. Yuping, L. H. Royden, D. Changrong, and X. Jiene (1992), The south Tibetan detachment system, Himalayan orogen: Extension contemporaneous with and parallel to shortening in a collisional mountain belt, *Spec. Pap. Geol. Soc. Am.*, *269*, 41 pp.

Burg, J. P. (1983), Tectogenese compare de deux segments de chaine de collision: Le sud du Tibet (suture du Tsangpo), la chaine hercynienne en Europe (suture du Massif Central), thesis, 450 pp., Univ. Montpellier II, Montpellier, France.

Chambers, J., R. Parrish, T. Argles, N. Harris, and M. Horstwood (2011), A short-duration pulse of ductile normal shear on the outer South Tibetan detachment in Bhutan: Alternating channel flow and critical taper mechanics of the eastern Himalaya, *Tectonics*, *30*, TC2005, doi:10.1029/2010TC002784.

Chapple, W. M. (1978), Mechanics of thin-skinned fold and thrust belts, *Geol. Soc. Am. Bull.*, *89*, 1189–1198, doi:10.1130/0016-7606(1978)89<1189:MOTFB>2.0.CO;2.

Clark, M. K., and R. Bilham (2008), Miocene rise of the Shillong Plateau and the beginning of the end for the Eastern Himalaya, *Earth Planet. Sci. Lett.*, *269*, 337–351, doi:10.1016/j.epsl.2008.01.045.

Clark, M. K., M. A. House, L. H. Royden, K. X. Whipple, B. C. Burchfiel, X. Zhang, and W. W. Tang (2005), Late Cenozoic uplift of southeastern Tibet, *Geology*, *33*, 525–528, doi:10.1130/G21265.1.

Cooper, F. J., B. A. Adams, C. S. Edwards, and K. V. Hodges (2012), Large normal-sense displacement on the South Tibetan fault system in the eastern Himalaya, *Geology*, doi:10.1130/G33318.1, in press.

Copley, A., J.-P. Avouac, and J.-Y. Royer (2010), India-Asia collision and the Cenozoic slowdown of the Indian plate: Implications for the forces driving plate motions, *J. Geophys. Res.*, *115*, B03410, doi:10.1029/2009JB006634.

Corrie, S. L., M. J. Kohn, N. McQuarrie, and S. P. Long (2012), Flattening the Bhutan Himalaya, *Earth Planet. Sci. Lett.*, *349–350*, 67–74, doi:10.1016/j.epsl.2012.07.001.

Craddock, W., E. Kirby, and H. Zhang (2011), Late Miocene-Pliocene range growth in the interior of the northeastern Tibetan Plateau, *Lithosphere*, *3*, 420–438, doi:10.1130/L159.1.

Daniel, C. G., L. S. Hollister, R. R. Parrish, and D. Grujic (2003), Exhumation of the Main Central Thrust from lower crustal depths, eastern Bhutan Himalaya, *J. Metamorph. Geol.*, *21*, 317–334, doi:10.1046/j.1525-1314.2003.00445.x.

Davidson, C., D. E. Grujic, L. S. Hollister, and S. M. Schmid (1997), Metamorphic reactions related to decompression and synkinematic intrusion of leucogranite, High Himalayan crystallines, Bhutan, *J. Metamorph. Geol.*, *15*, 593–612, doi:10.1111/j.1525-1314.1997.tb00638.x.

Davis, D., J. Suppe, and F. A. Dahlen (1983), Mechanics of fold-and-thrust belts and accretionary wedges, *J. Geophys. Res.*, *88*, 1153–1172, doi:10.1029/JB088iB02p01153.

DeCelles, P. G. (1994), Late Cretaceous-Paleocene synorogenic sedimentation and kinematic history of the Sevier thrust belt, northeast Utah and southwest Wyoming, *Geol. Soc. Am. Bull.*, *106*, 32–56, doi:10.1130/0016-7606(1994)106<0032:LCPSSA>2.3.CO;2.

DeCelles, P. G., D. M. Robinson, and G. Zandt (2002), Implications of shortening in the Himalayan fold-thrust belt for uplift of the Tibetan Plateau, *Tectonics*, *21*(6), 1062, doi:10.1029/2001TC001322.

Edwards, M. A., W. S. F. Kidd, L. Jixiang, Y. Yue, and M. Clark (1996), Multi-stage development of the southern Tibetan detachment system near Khula Kangri; New data from Gonto La, *Tectonophysics*, *260*, 1–19, doi:10.1016/0040-1951(96)00073-X.

Ehlers, T. A., and K. A. Farley (2003), Apatite (U-Th)/He thermochronometry: Methods and applications to problems in tectonic and surface processes, *Earth Planet. Sci. Lett.*, *206*, 1–14, doi:10.1016/S0012-821X(02)01069-5.

Ehlers, T. A., et al. (2005), Computational tools for low-temperature thermochronometer interpretation, in *Low-Temperature Thermochronology: Techniques, Interpretations, and Applications*, edited by P. W. Reiners and T. A. Ehlers, *Rev. Mineral. Geochem.*, *58*, 589–622, doi:10.2138/rmg.2005.58.22.

Flowers, R. M., R. A. Ketcham, D. L. Shuster, and K. A. Farley (2009), Apatite (U-Th)/He thermochronometry using a radiation damage accumulation and annealing model, *Geochim. Cosmochim. Acta*, *73*, 2347–2365, doi:10.1016/j.gca.2009.01.015.

Gansser, A. (1964), *Geology of the Himalayas*, 289 pp., Wiley-Interscience, New York.

Gansser, A. (1983), *Geology of the Bhutan Himalaya*, 181 pp., Birkäuser, Basel.

Gehrels, G. E., P. G. DeCelles, A. Martin, T. P. Ojha, and G. Pinhassi (2003), Initiation of the Himalayan Orogen as an early Paleozoic thin-skinned thrust belt, *GSA Today*, *13*, 4–9, doi:10.1130/1052-5173(2003)13<4:IOTHOA>2.0.CO;2.

Grujic, D., L. S. Hollister, and R. R. Parrish (2002), Himalayan metamorphic sequence as an orogenic channel: Insight from Bhutan, *Earth Planet. Sci. Lett.*, *198*, 177–191, doi:10.1016/S0012-821X(02)00482-X.

Grujic, D., I. Coutand, B. Bookhagen, S. Bonnet, A. Blythe, and C. Duncan (2006), Climatic forcing of erosion, landscape, and tectonics in the Bhutan Himalayas, *Geology*, *34*, 801–804, doi:10.1130/G22648.1.

Grujic, D., C. J. Warren, and J. L. Wooden (2011), Rapid synconvergent exhumation of Miocene-aged lower and orogenic crust in the eastern Himalaya, *Lithosphere*, *3*, 346–366, doi:10.1130/L154.1.

Guenthner, W., P. W. Reiners, R. A. Ketcham, and L. Nasdala (2011), Development of a radiation damage and annealing model for the zircon (U-Th)/He thermchronometer, Abstract V23A-2550 presented at 2011 Fall Meeting, AGU, San Francisco, Calif., 5–9 Dec.

Hames, W. E., and S. A. Bowring (1994), An empirical evaluation of the argon diffusion geometry in muscovite, *Earth Planet. Sci. Lett.*, *124*, 161–169, doi:10.1016/0012-821X(94)00079-4.

Hauck, M. L., K. D. Nelson, W. Brown, W. Zhao, and A. R. Ross (1998), Crustal structure of the Himalayan orogen at ~90°E longitude from Project INDEPTH deep reflection profiles, *Tectonics*, *17*, 481–500, doi:10.1029/98TC01314.

Heim, A., and A. Gansser (1939), Central Himalayas—Geological observations of Swiss expedition, 1936, *Mem. Soc. Helv. Sci. Nat.*, *73*, 1–245.

Herman, F., J. Braun, and W. Dunlap (2007), Tectonomorphic scenarios in the Southern alps of New Zealand, *J. Geophys. Res.*, *112*, B04201, doi:10.1029/2004JB003472.

Herman, F., et al. (2010), Exhumation, crustal deformation, and thermal structure of the Nepal Himalaya derived from the inversion of thermochronological and thermobarometric data and modeling of the topography, *J. Geophys. Res.*, *115*, B06407, doi:10.1029/2008JB006126.

Hodges, K. V. (2000), Tectonics of the Himalaya and southern Tibet from two perspectives, *Geol. Soc. Am. Bull.*, *112*, 324–350, doi:10.1130/0016-7606(2000)112<324:TOTHAS>2.0.CO;2.

Hollister, L. S., and D. Grujic (2006), Pulsed channel flow in Bhutan, *Geol. Soc. Spec. Publ.*, *268*, 415–423, doi:10.1144/GSL.SP.2006.268.01.19.

Kellett, D. A., and D. Grujic (2012), New insight into the Southern Tibetan detachment system: Not a single progressive deformation, *Tectonics*, *31*, TC2007, doi:10.1029/2011TC002957.

Kellett, D. A., D. Grujic, and S. Erdmann (2009), Miocene structural reorganization of the South Tibetan detachment, eastern Himalaya: Implications for continental collision, *Lithosphere*, *1*, 259–281, doi:10.1130/L56.1.

Kellett, D. A., D. Grujic, C. J. Warren, J. Cottle, R. A. Jamieson, and T. Tenzin (2010), Metamorphic history of a syn-convergent orogen-parallel detachment: The South Tibetan detachment system, Bhutan Himalaya, *J. Metamorph. Geol.*, *28*, 785–808, doi:10.1111/j.1525-1314.2010.00893.x.

Ketcham, R. A., R. A. Donelick, and W. D. Carlson (1999), Variability of apatite fission-track annealing kinetics; III, Extrapolation to geological time scales, *Am. Mineral.*, *84*, 1235–1255.

Kohn, M. J., M. S. Wieland, C. D. Parkinson, and B. N. Upreti (2004), Miocene faulting at plate tectonic velocity in the Himalaya of central Nepal, *Earth Planet. Sci. Lett.*, *228*, 299–310, doi:10.1016/j.epsl.2004.10.007.

Larson, K. M., R. Burgmann, R. Bilham, and J. Freymueller (1999), Kinematics of the India-Eurasia collision zone from GPS measurements, *J. Geophys. Res.*, *104*, 1077–1093, doi:10.1029/1998JB900043.

Laslett, G. M., P. F. Green, I. R. Duddy, and A. J. W. Gleadow (1987), Thermal annealing of fission tracks in apatite: 2, A quantitative analysis, *Chem. Geol.*, *65*, 1–13, doi:10.1016/0168-9622(87)90057-1.

Lavé, J., and J. P. Avouac (2000), Active folding of fluvial terraces across the Siwaliks Hills, Himalayas of central Nepal, *J. Geophys. Res.*, *105*, 5735–5770, doi:10.1029/1999JB900292.

Lease, R. O., D. W. Burbank, M. K. Clark, K. A. Farley, D. Zhang, and H. Zhang (2011), Middle Miocene reorganization of deformation along the northeastern Tibetan Plateau, *Geology*, *39*, 359–362, doi:10.1130/G31356.1.

LeFort, P. (1975), Himalayas: The collided range. Present knowledge of the continental arc, *Am. J. Sci.*, *275A*, 1–44.

Long, S., and N. McQuarrie (2010), Placing limits on channel flow: Insights from the Bhutan Himalaya, *Earth Planet. Sci. Lett.*, *290*, 375–390, doi:10.1016/j.epsl.2009.12.033.

Long, S., N. McQuarrie, T. Tobgay, C. Rose, G. Gehrels, and D. Grujic (2011a), Tectonostratigraphy of the Lesser Himalaya of Bhutan: Implications for the along-strike stratigraphic continuity of the northern Indian margin, *Geol. Soc. Am. Bull.*, *123*, 1406–1426, doi:10.1130/B30202.1.

Long, S., N. McQuarrie, T. Tobgay, and D. Grujic (2011b), Geometry and crustal shortening of the Himalayan fold-thrust belt, eastern and central Bhutan, *Geol. Soc. Am. Bull.*, *123*, 1427–1447, doi:10.1130/B30203.1.

Long, S., N. McQuarrie, T. Tobgay, and J. Hawthorne (2011c), Quantifying internal strain and deformation temperature in the eastern Himalaya, Bhutan: Implications for the evolution of strain in thrust sheets, *J. Struct. Geol.*, *33*, 579–608, doi:10.1016/j.jsg.2010.12.011.

Long, S. P., N. McQuarrie, T. Tobgay, D. Grujic, and L. Hollister (2011d), Geologic map of Bhutan, *J. Maps*, *7*, 184–192, doi:10.4113/jom.2011.1159.

Mancktelow, N. S., and B. Grasemann (1997), Time-dependent effects of heat advection and topography on cooling histories during erosion, *Tectonophysics*, *270*, 167–195, doi:10.1016/S0040-1951(96)00279-X.

Mattauer, M. (1986), Intracontinental subduction, crust-mantle décollemont and crustal-stacking wedge in the Himalayas and other collision belts, in *Collision Tectonics*, edited by M. P. Coward and A. C. Ries, *Geol. Soc. Spec. Publ.*, *19*, 37–50, doi:10.1144/GSL.SP.1986.019.01.02.

McQuarrie, N., D. Robinson, S. Long, T. Tobgay, D. Grujic, G. Gehrels, and M. Ducea (2008), Preliminary stratigraphic and structural architecture of Bhutan: Implications for the along-strike architecture of the Himalayan system, *Earth Planet. Sci. Lett.*, *272*, 105–117, doi:10.1016/j.epsl.2008.04.030.

Mitra, G. (1994), Strain variation in thrust sheets across the Sevier fold-and-thrust belt (Idaho-Utah-Wyoming): Implications for section restoration and wedge taper evolution, *J. Struct. Geol.*, *16*, 585–602, doi:10.1016/0191-8141(94)90099-X.

Mitra, S., K. Priestley, A. K. Bhattacharyya, and V. K. Gaur (2005), Crustal structure and earthquake focal depths beneath northeastern India and southern Tibet, *Geophys. J. Int.*, *160*, 227–248, doi:10.1111/j.1365-246X.2004.02470.x.

Mugnier, J.-L., and P. Huyghe (2006), Ganges basin geometry records a pre-15 Ma isostatic rebound of Himalaya, *Geology*, *34*, 445–448, doi:10.1130/G22089.1.

Mugnier, J.-L., P. Huyghe, P. Leturmy, and F. Jouanne (2004), Episodicity and rates of thrust sheet motion in the Himalayas (western Nepal), in *Thrust Tectonics and Hydrocarbon Systems*, edited by K. R. McClay, *AAPG Mem.*, *82*, 91–114.

Ni, J., and M. Barazangi (1984), Seismotectonics of the Himalayan collision zone: Geometry of the under-thrusting Indian plate beneath the Himalaya, *J. Geophys. Res.*, *89*, 1147–1163, doi:10.1029/JB089iB02p01147.

Pandey, M. R., R. P. Tandukar, J. P. Avouac, J. Vergne, and T. Heritier (1999), Seismotectonics of the Nepal Himalaya from a local seismic network, *J. Asian Earth Sci.*, *17*, 703–712, doi:10.1016/S1367-9120(99)00034-6.

Platt, J. P. (1986), Dynamics of orogenic wedges and the uplift of high-pressure metamorphic rocks, *Geol. Soc. Am. Bull.*, *97*, 1037–1053, doi:10.1130/0016-7606(1986)97<1037:DOOWAT>2.0.CO;2.

Powell, C. M., and P. J. Conaghan (1973), Plate tectonics and the Himalayas, *Earth Planet. Sci. Lett.*, *20*, 1–12, doi:10.1016/0012-821X(73)90134-9.

Ray, L., A. Bhattacharya, and S. Roy (2007), Thermal conductivity of Higher Himalayan Crystallines from Garhwal Himalaya, India, *Tectonophysics*, *434*, 71–79, doi:10.1016/j.tecto.2007.02.003.

Reiners, P. W., and M. T. Brandon (2006), Using thermochronology to understand orogenic erosion, *Annu. Rev. Earth Planet. Sci.*, *34*, 419–466, doi:10.1146/annurev.earth.34.031405.125202.

Reiners, P. W., T. L. Spell, S. Nicolescu, and K. A. Zanetti (2004), Zircon (U-Th)/He thermochronometry: He diffusion and comparisons with $^{40}Ar/^{39}Ar$ dating, *Geochim. Cosmochim. Acta*, *68*, 1857–1887, doi:10.1016/j.gca.2003.10.021.

Robinson, D. M., P. G. DeCelles, and P. Copeland (2006), Tectonic evolution of the Himalayan thrust belt in western Nepal: Implications for channel flow models, *Geol. Soc. Am. Bull.*, *118*, 865–885, doi:10.1130/B25911.1.

Sak, P. B., N. McQuarrie, B. P. Oliver, N. Lavdovsky, and M. S. Jackson (2012), Unraveling the central Appalachian fold-thrust belt, Pennsylvania: The power of sequentially restored balanced cross sections for a blind fold-thrust belt, *Geosphere*, *8*, 685–702, doi:10.1130/GES00676.1.

Stipp, M., H. Stunitz, R. Heilbronner, and S. M. Schmid (2002), The eastern Tonale fault zone: A 'natural laboratory' for crystal plastic deformation over a temperature range from 250° to 700°C, *J. Struct. Geol.*, *24*, 1861–1884, doi:10.1016/S0191-8141(02)00035-4.

Stocklin, J. (1980), Geology of Nepal and its regional frame, *J. Geol. Soc.*, *137*, 1–34, doi:10.1144/gsjgs.137.1.0001.

Stüwe, K., and D. Foster (2001), $^{40}Ar/^{39}Ar$, pressure, temperature and fission track constraints on the age and nature of metamorphism around the Main Central Thrust in the eastern Bhutan Himalaya, *J. Asian Earth Sci.*, *19*(1–2), 85–95, doi:10.1016/S1367-9120(00)00018-3.

Swapp, S. M., and L. S. Hollister (1991), Inverted metamorphism within the Tibetan slab of Bhutan: Evidence for a tectonically transported heat source, *Can. Mineral.*, *29*, 1019–1041.

Thiede, R. C., T. A. Ehlers, B. Bookhagen, and M. R. Strecker (2009), Erosional variability along the northwest Himalaya, *J. Geophys. Res.*, *114*, F01015, doi:10.1029/2008JF001010.

Tobgay, T., N. McQuarrie, S. Long, M. J. Kohn, and S. Corrie (2012), The age and rate of displacement along the Main Central Thrust in the western Bhutan Himalaya, *Earth Planet. Sci. Lett.*, *319-320*, 146–158, doi:10.1016/j.epsl.2011.12.005.

van Hinsbergen, D. J. J., B. Steinberger, P. V. Doubrovine, and R. Gassmoller (2011), Acceleration and deceleration of India–Asia convergence since the Cretaceous: Roles of mantle plumes and continental collision, *J. Geophys. Res.*, *116*, B06101, doi:10.1029/2010JB008051.

Warren, C. J., D. Grujic, D. A. Kellett, J. Cottle, R. A. Jamieson, and K. S. Ghalley (2011), Probing the depths of the India-Asia collision: U-Th-Pb monazite chronology of granulites from NW Bhutan, *Tectonics*, *30*, TC2004, doi:10.1029/2010TC002738.

Warren, C. J., D. Grujic, J. Cottle, and N. W. Rogers (2012), Constraining cooling histories: Rutile and titanite chronology and diffusion modeling in NW Bhutan, *J. Metamorph. Geol.*, *30*, 113–130, doi:10.1111/j.1525-1314.2011.00958.x.

Whipp, D. M., T. A. Ehlers, A. E. Blythe, K. W. Huntington, K. V. Hodges, and D. W. Burbank (2007), Plio-Quaternary exhumation history of the central Nepalese Himalaya: 2. Thermokinematic and thermochronometer age prediction model, *Tectonics*, *26*, TC3003, doi:10.1029/2006TC001991.

Whynot, N., D. Grujic, S. Long, and N. McQuarrie (2010), Apparent temperature gradient across the Lesser Himalayan Sequence: Raman spectroscopy on carbonaceous material in the eastern Bhutan Himalaya, in *Proceedings for the 25th Himalaya-Karakoram Tibet Workshop, San Francisco, California, U.S.A.*, edited by M. L. Leech, S. L. Klemperer, and W. D. Mooney, *U.S. Geol. Surv. Open File Rep.*, *2010-1099*, 2 pp. [Available at http://pubs.usgs.gov/of/2010-1099/whynot/.]

Yin, A. (2006), Cenozoic tectonic evolution of the Himalayan orogen as constrained by along-strike variation of structural geometry, exhumation history, and foreland sedimentation, *Earth Sci. Rev.*, *76*, 1–131, doi:10.1016/j.earscirev.2005.05.004.

Yonkee, A., and A. B. Weil (2010), Reconstructing the kinematic evolution of curved mountain belts: Internal strain patterns in the Wyoming salient, Sevier thrust belt, U.S.A, *Geol. Soc. Am. Bull.*, *122*, 24–49, doi:10.1130/B26484.1.

Zhang, P. Z., et al. (2004), Continuous deformation of the Tibetan Plateau from global positioning system data, *Geology*, *32*, 809–812, doi:10.1130/G20554.1.

Zheng, D., P. Z. Zhang, J. L. Wan, D. Y. Yuan, C. Y. Li, G. M. Yin, G. L. Zhang, Z. C. Wang, W. Min, and J. Chen (2006), Rapid exhumation at ~8 Ma on the Liupan Shan thrust fault from apatite fission-track thermochronology: Implications for growth of the northeastern Tibetan Plateau margin, *Earth Planet. Sci. Lett.*, *248*, 198–208, doi:10.1016/j.epsl.2006.05.023.